

# Design and Characterization of a Full-Duplex Multiantenna System for WiFi Networks

Melissa Duarte, *Member, IEEE*, Ashutosh Sabharwal, *Senior Member, IEEE*, Vaneet Aggarwal, *Member, IEEE*, Rittwik Jana, *Member, IEEE*, K. K. Ramakrishnan, *Fellow, IEEE*, Christopher W. Rice, and N. K. Shankaranarayanan, *Senior Member, IEEE*

**Abstract**—In this paper, we present an experiment- and simulation-based study to evaluate the use of full duplex (FD) as a potential mode in practical IEEE 802.11 networks. To enable the study, we designed a 20-MHz multiantenna orthogonal frequency-division-multiplexing (OFDM) FD physical layer and an FD media access control (MAC) protocol, which is backward compatible with current 802.11. Our extensive over-the-air experiments, simulations, and analysis demonstrate the following two results. First, the use of multiple antennas at the physical layer leads to a higher ergodic throughput than its hardware-equivalent multiantenna half-duplex (HD) counterparts for SNRs above the median SNR encountered in practical WiFi deployments. Second, the proposed MAC translates the physical layer rate gain into near doubling of throughput for multinode single-AP networks. The two results allow us to conclude that there are potentially significant benefits gained from including an FD mode in future WiFi standards.

**Index Terms**—Full-duplex, media access control (MAC), orthogonal frequency-division multiplexing (OFDM), WiFi, 802.11.

## I. INTRODUCTION

CURRENTLY deployed wireless networks cannot transmit and receive on the same frequency band at the same time. As a result, networks are either time-division duplex (e.g., WiFi) or frequency-division duplex (e.g., cellular). The key challenge in achieving true full-duplex (FD) communication is the large power differential between the “self-interference” created by a node’s own radio transmission and the signal of interest originating from a distant node. The large power differential is simply because the self-interference signal travels much shorter distances compared with the signal of interest. As a result of the large power differential, the signal of interest is

swamped by the self-interference in digital baseband (BB) due to finite resolution of analog-to-digital conversion.

FD experimental demonstration for narrow-band systems was first reported in 1998 [1]. Since then, multiple authors [2]–[11] have reported different methods and implementations for various single- and multiple-antenna extensions. However, to date, none of the prior methods have reported experimental evidence to achieve long-enough communication ranges (best reported number in open literature is 8 m with line-of-sight) for FD to be considered in WiFi-like systems. Our focus in this paper is to investigate if a practical WiFi system can leverage FD gains for its typical communication range.

In this paper, we present a multiantenna wideband physical layer (PHY) and media access control (MAC) design to enable a practical FD mode in WiFi. Our experiment-based analysis is the first to investigate the performance of FD systems over the entire range of SNR values typical in WiFi communications. Via extensive over-the-air tests, we show that our design achieves higher throughputs than its hardware-equivalent half-duplex (HD) multiple-input–multiple-output (MIMO) counterparts for a significant portion of the WiFi communication range. Our contributions in design are twofold. First, to reduce the self-interference, the PHY uses a combination of three methods: 1) passive suppression (PS) via appropriate placement of multiple antennas on a device; 2) a per-subcarrier per-receive-antenna analog self-interference canceler for MIMO orthogonal frequency-division-multiplexing (OFDM) systems; and 3) a digital self-interference canceler implemented in BB. Second, to gauge realistic gains in actual systems, the MAC design leverages legacy WiFi request-to-send (RTS)/clear-to-send (CTS) packets to seamlessly support legacy HD and new FD modes. By design, the MAC is minimally different from IEEE 802.11 [26] and is designed to leverage the existing 802.11 ecosystem to accelerate potential adoption of the FD mode in future 802.11 revisions.

*En route* to showing that our design provides throughput gains for WiFi networks, we perform extensive statistical characterization of the design elements, revealing several new findings. Our findings can be divided into three categories: 1) self-interference canceler performance in FD; 2) the comparison of empirical ergodic rates (ERs) achieved by FD and HD systems; and 3) an extensive MAC layer performance analysis for different traffic scenarios.

**Results on Self-Interference Cancellation in FD:** Recall that we are employing three serially concatenated mechanisms to reduce self-interference. To understand the role and interaction

Manuscript received October 8, 2012; revised March 1, 2013 and July 23, 2013; accepted September 25, 2013. Date of publication November 5, 2013; date of current version March 14, 2014. The review of this paper was coordinated by Dr. J. Pan. The work of M. Duarte and A. Sabharwal was supported in part by a Roberto Rocca Fellowship and in part by the National Science Foundation under Grant CNS-0923479, Grant CNS-1012921, and Grant CNS-1161596.

M. Duarte was with Rice University, Houston, TX 77251 USA. She is now with the Swiss Federal Institute of Technology, 1015 Lausanne, Switzerland (e-mail: melissaduarte@alumni.rice.edu).

A. Sabharwal is with the Department of Electrical and Computer Engineering, Rice University, Houston, TX 77005 USA (e-mail: ashu@rice.edu).

V. Aggarwal, R. Jana, K. K. Ramakrishnan, C. W. Rice, and N. K. Shankaranarayanan are with AT&T Labs Research, Florham Park, NJ 07932 USA (e-mail: vaneet@research.att.com; rjana@research.att.com; kkrama@research.att.com; cwrice@research.att.com; shankar@research.att.com).

Color versions of one or more of the figures in this paper are available online at <http://ieeexplore.ieee.org>.

Digital Object Identifier 10.1109/TVT.2013.2284712

of each cancelation stage, we show the following four results experimentally for 20-MHz 64-subcarrier OFDM.

First, we consider antenna placement for  $2 \times 1$  multiple-input–single-output (MISO) FD, where each node has three antennas, i.e., two transmit and one receive. By placing antennas *around* the device to use the device itself to attenuate self-interference and leverage antenna polarization, self-interference can be suppressed by an additional 15 dB compared with the configuration where there is no device. Thus, the key message is that antenna placement is crucial in FD devices. We note that our antenna placement aims to only increase the path loss of self-interference and thus can be used for all device sizes. However, the suppression obtained with the antenna placement is device dependent. In contrast, prior antenna placement techniques aim to create beamforming nulls [5], [10], [11], which require fixed antenna spacing inherently assuming that the self-interference channel does not have multipath components.

Second, passive device-based suppression largely reduces the direct line-of-sight path for self-interference, and thus, the multipath reflections become dominant. As a result, with more passive cancelation, the self-interference channel becomes more frequency selective. The measured frequency selectivity was our motivation behind per-subcarrier analog canceler, which actively cancels self-interference in each OFDM band with subband-specific cancelation coefficients (unlike prior works, e.g., [5] and [7]).

Third, we measure the performance of each cancelation stage and also consider its impact on subsequent stages. The measured results clearly show that more cancelation by one stage means lower cancelation by subsequent stages. As a result, the performance of each stage is *not* independent of the performance of the stages prior to it. Thus, our results show that, for our experimental testbed, the total self-interference canceled by any two concatenated stages is *not* the sum of maximum self-interference canceled by each stage individually in isolation. We note that in [5], it was assumed that the performance of cancelation stages is additive to obtain an estimate of 73 dB of total analog plus digital cancelation (DC). However, the prototype implemented in [5] achieved 30 dB of analog plus DC, which is 43 dB less than their estimated maximum.

Last, we combine all three methods of cancelation (i.e., passive, analog, and digital) and demonstrate that our three-stage self-cancelation system achieves a median cancelation of 85 dB, with a minimum of 70 dB and a maximum of 100 dB. The median and maximum numbers for *total* self-interference cancelation are the best reported numbers in the open literature to date.

**Main Result on ER Comparisons:** We implemented two FD physical layers, i.e.,  $2 \times 1$  MISO and  $1 \times 1$  single-input–single-output (SISO), and three HD systems, i.e.,  $2 \times 1$  MISO,  $3 \times 1$  MISO, and  $2 \times 2$  MIMO. The RF hardware usage of the five systems is compared by counting the *total* number of RF upconversion and downconversion chains. A  $2 \times 2$  MIMO HD system uses two upconverting and two downconverting chains for a total of four chains. A  $2 \times 1$  MISO FD system uses three upconverting and one downconverting chains, again for a total of four chains. Similarly, all other configurations

previously mentioned use four or fewer total chains. The main motivation for using RF hardware equivalence is that the power consumption of RF is a key factor and often determines the largest supported antenna configurations.

We perform extensive experiments, which allow us to compare the performance of FD and HD systems for SNR values from 0 to 40 dB; note that WiFi standards nominally target SNR range of 10–30 dB. We observe that, for SNR larger than 20 dB,  $2 \times 1$  FD often achieves higher ERs than the rest of the four configurations.

**Results on MAC Layer:** Recall that a primary design objective for the MAC was to make minimal changes to legacy 802.11 MAC to expedite adoption of FD. Thus, the MAC design supports both legacy HD and FD flows without hurting the throughput for HD nodes significantly. For the FD flows, asymmetric packet sizes are also supported since the packet sizes in the two directions of an FD transfer may be different.

Our results were obtained in four major steps. First, we evaluated the performance of a single access point (AP) communicating with one FD flow as a function of packet asymmetry, which is the difference in packet sizes of uplink and downlink of an FD transfer. The packet sizes ranged from 40-byte Transmission Control Protocol (TCP) acknowledgements (ACKs) to 1500-byte data packets. For different levels of packet size asymmetry, the throughput gains ranged from 30% to 100% compared with a legacy HD system *with* RTS/CTS and from 18% to 87% compared with a legacy HD system *without* RTS/CTS.

Second, we considered scaling of an FD system as one AP communicates with more FD nodes. We find that the sum throughput for an FD system increases by a factor of at least two, when compared with an HD system with RTS/CTS with the same number of nodes.

Third, to understand the dynamics of coexistence, we first consider the system performance when FD nodes coexist with HD nodes, where the HD nodes' MAC logic has been slightly “modified” to ignore collisions during an FD transfer. For a system with  $m$  FD and  $m$  HD nodes, the total throughput compared with an HD-only system (with  $2m$  nodes) increases by a factor of  $1 + m/(2m + 1)$ . The percentage increase in throughput for a mixed system compared with that for an HD system increases with  $m$  such that the maximum percentage increase can be up to 50%. The uplink and downlink throughputs of both FD and HD nodes in a mixed system are higher, as compared with those in an HD system with  $2m$  HD nodes.

Finally, we consider the coexistence with legacy HD nodes that have no modifications. Much like the previous discussion, the uplink and downlink throughputs of FD nodes increase, and so does the downlink throughput to HD nodes, as compared with a purely HD system. However, HD nodes do not grab the channel as often as they would in a purely HD system (with the same total number of nodes) leading to a decrease in their uplink throughput by around 40% for  $m = 2$ , as compared with a purely HD system. To rectify this situation, we change the proposed FD MAC design to provide channel access fairness among all FD and HD users at a small cost to throughput. This change in FD MAC decreases throughput by around 2% for the FD nodes (as compared with the case of modified HD and unchanged FD nodes) by making them less aggressive in lieu

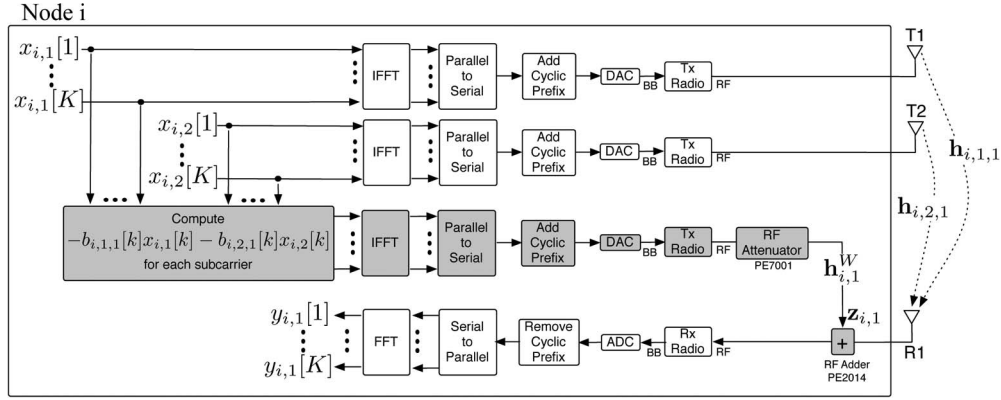


Fig. 1. Block diagram of an FD OFDM node with two transmitter antennas and one receiver antenna ( $2 \times 1$ ) using PS and active analog self-interference cancellation. Blocks used for active AC are highlighted in gray. PS consists in propagation loss through  $\mathbf{h}_{i,1,1}$  and  $\mathbf{h}_{i,2,1}$ . The Tx Radios are radio chains that upconvert from BB to RF. The Rx radios are radio chains that downconvert from RF to BB.

of increased probability of access for legacy HD nodes, which is almost the same as if all the nodes were HD.

The rest of this paper is organized as follows. In Section II, we describe the MIMO wideband canceler design, which uses a combination of PS and active cancellation techniques. In Section III, we describe the experimental setup for validating the design. Sections IV and V evaluate the cancellation design in terms of cancellation and rate, respectively. In Section VI, we give our MAC design with detailed evaluations in Section VII. Section VIII concludes this paper.

## II. MULTIPLE-INPUT-MULTIPLE-OUTPUT WIDEBAND CANCELER DESIGN

We present a design for a wideband multiple-antenna self-interference canceler, which uses a combination of PS and active cancellation techniques, where PS precedes active cancellation. The cancellation techniques are explained as follows.

**PS:** PS is achieved by maximizing the attenuation of the self-interference signal due to propagation path loss over the self-interference channel, which is the channel between same node transmitter and receiver antennas. The amount of PS depends on the distance between antennas, the antenna directionality, and the antenna placement on the FD device. We use  $\mathbf{h}_{i,m,n}$  to denote the self-interference channel between the transmitter antenna  $m$  and receiver antenna  $n$  at node  $i$ . The self-interference channel  $\mathbf{h}_{i,m,n}$  varies with time and frequency due to changes in the node's environment. Our design of self-interference cancellation for OFDM systems will be presented in the frequency domain. We use  $h_{i,m,n}[k]$  to denote the magnitude and phase that the self-interference channel  $\mathbf{h}_{i,m,n}$  applies to subcarrier  $k$ . For a system with  $K$  subcarriers, the channel vector is defined as  $\mathbf{h}_{i,m,n} = [h_{i,m,n}[1], h_{i,m,n}[2], \dots, h_{i,m,n}[K]]$ . Fig. 1 shows the two passive cancellation paths  $\mathbf{h}_{i,1,1}$  and  $\mathbf{h}_{i,2,1}$  for an FD node with two transmitter antennas and one receiver antenna.

**Active AC:** As the name suggests, the active cancellation is performed in an analog domain *before* the received signal passes through the analog-to-digital converter (ADC). For an OFDM MIMO node, the self-interference signal received at node  $i$  antenna  $n$  on subcarrier  $k$  after PS is equal to

$y_{i,n}^{\text{PS}}[k] = \sum_{m=1}^M h_{i,m,n}[k]x_{i,m}[k]$ , where  $x_{i,m}[k]$  is the signal transmitted from node  $i$  on subcarrier  $k$  antenna  $m$ . Analog cancellation (AC) of the self-interference at receiver antenna  $n$  is implemented by subtracting an estimate of  $y_{i,n}^{\text{PS}}[k]$  from the received signal.

In our proposed MIMO wideband canceler design, the additional hardware components required for active AC of the self-interference at one receiver antenna consist of one digital-to-analog converter (DAC), one upconverting radio chain (Tx Radio) that upconverts the signal from BB to RF, one fixed attenuator, and one RF adder. Fig. 1 shows a diagram of our proposed AC for an FD node with two transmitter antennas and one receiver antenna. One input to the RF adder is the signal at the receiver antenna, and the other input is a canceling signal  $\mathbf{z}_{i,n}$  local to node  $i$ , which is input to the RF adder via a wire. For subcarrier  $k$  and receiver antenna  $n$ , the local signal  $\mathbf{z}_{i,n}$  is equal to  $z_{i,n}[k] = -h_{i,n}^W[k] \sum_{m=1}^M b_{i,m,n}[k]x_{i,m}[k]$ , where  $h_{i,n}^W[k]$  denotes the magnitude and phase that affect a signal at subcarrier  $k$  when passing through the wire connected to the RF adder at node  $i$  receiver antenna  $n$ . Furthermore,  $b_{i,m,n}[k]$  denotes the cancellation coefficient for the self-interference received at antenna  $n$  from transmitter antenna  $m$  at subcarrier  $k$  at node  $i$ .

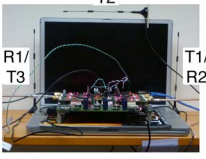
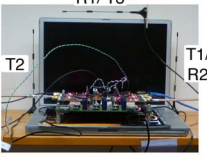
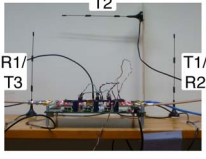
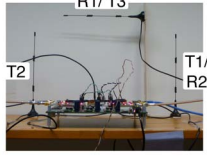
The self-interference at subcarrier  $k$  after AC at antenna  $n$  (this is the signal at the output of the RF adder connected to antenna  $n$ ) is equal to  $y_{i,n}^{\text{AC}}[k] = y_{i,n}^{\text{PS}}[k] - z_{i,n}[k]$ , which can be rewritten as  $y_{i,n}^{\text{AC}}[k] = \sum_{m=1}^M (h_{i,m,n}[k] - h_{i,n}^W[k]b_{i,m,n}[k])x_{i,m}[k]$ . From the equation for  $y_{i,n}^{\text{AC}}[k]$ , we observe that active AC achieves perfect cancellation when  $b_{i,m,n}[k] = h_{i,m,n}[k]/h_{i,n}^W[k]$ . In a real system,  $h_{i,m,n}[k]$  and  $h_{i,n}^W[k]$  can only be estimated, which leads to the following computation of:

$$b_{i,m,n}[k] = \hat{h}_{i,m,n}[k]/\hat{h}_{i,n}^W[k] \quad (1)$$

where  $\hat{h}_{i,m,n}[k]$  and  $\hat{h}_{i,n}^W[k]$  are the estimates of  $h_{i,m,n}[k]$  and  $h_{i,n}^W[k]$ , respectively. Thus, cancellation is usually not perfect. The estimates of  $h_{i,m,n}[k]$  and  $h_{i,n}^W[k]$  are computed based on pilots sent from each transmitter radio on orthogonal time slots.



TABLE I  
DIFFERENT ANTENNA CONFIGURATIONS WITH DISTANCE BETWEEN  
PARALLEL ANTENNAS OF 37.5 cm

	Antenna Placement 1 (A1)	Antenna Placement 2 (A2)
	T2 is orthogonal to T1/R2 R1/T3 is parallel to T1	T2 is parallel to T1/R2 R1/T3 is orthogonal to T1
With Device		
No Device		

In a WiFi system that uses RTS/CTS, the estimates of  $h_{i,m,n}[k]$  and  $h_{i,n}^W[k]$  can be computed based on pilots sent during the RTS/CTS transmissions. Furthermore, since  $h_{i,n}^W[k]$  is a wire, it is a static channel and it does not need to be estimated often. While the RTS/CTS packet exchange adds overhead to the system, it enables FD and results in overall rate gains, as will be shown in Sections VI and VII.

We note that any additional transmitter radio used for AC does not require a power amplifier since it is transmitting over a wire. However, for our specific implementation, the radio used for AC had a power amplifier, which could not be removed. Hence, we used a fixed RF attenuator connected in series, as shown in Fig. 1, to reduce the signal power levels at the output of the canceler radio to the levels required for cancellation. The attenuator used was a passive device (part number PE7001 [12]) that attenuates all the frequencies in the band of interest by the same amount. The value set for the attenuator was a function of the antenna configuration used because different antenna configurations resulted in different levels of self-interference power at the receiver antenna; different antenna configurations have different amounts of PS, as will be shown in Section IV-B. The four antenna configurations used are shown in Table I and will be explained in more detail in Section III-C. The attenuator was set equal to 35 dB for Antenna Placement 1 (A1) without device, 45 dB for A1 with device, 50 dB for Antenna Placement 2 (A2) without device, and 55 dB for A2 with device. The RF attenuator would not have been needed if the radio used for AC had a larger range of output power values and did not use a power amplifier by default.

We highlight that the RF adder used for AC is a passive device (part number PE2014 [13]) and applies the same addition operation to all the frequencies in the band of interest.

DC: There is residual self-interference  $y_{i,n}^{AC}[k]$  that remains after AC due to imperfect AC. Active DC estimates  $y_{i,n}^{AC}[k]$  and subtracts this estimate from the received signal in the digital domain. The estimate of  $y_{i,n}^{AC}[k]$  is computed based on a second round of pilots sent from each transmitter antenna and received while applying AC to each receiver antenna. Specifically, the second round of pilots is used to compute  $h_{i,m,n}[k]$  —

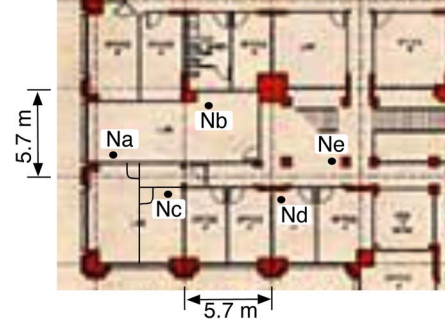


Fig. 2. Setup locations of nodes.

TABLE II  
LINKS CONSIDERED IN EXPERIMENTS. ALL LINKS EXCEPT LINK 1  
ARE NON-LINE OF SIGHT

Link number	Node pair	Physical Distance	Walls crossed
1	Na, Nb	6.5 m	0
2	Nd, Ne	4.4 m	1
3	Nb, Ne	9.3 m	1
4	Nc, Ne	11.3 m	1
5	Na, Ne	14.8 m	1
6	Nb, Nc	6.5 m	2
7	Nb, Nd	8.3 m	2
8	Na, Nc	4.7 m	3
9	Nc, Nd	8.2 m	3
10	Na, Nd	12.7 m	3

$h_{i,n}^W[k]b_{i,m,n}[k]$ . Alternatively, the estimate of  $y_{i,n}^{AC}[k]$  can be computed without extra pilots if implemented based on correlation between the transmitted and received self-interference payload signals.

### III. PHYSICAL LAYER EXPERIMENT DESCRIPTION

Here, we describe our experiment testbed, antenna configurations, and physical layer techniques, which will be compared, as well as their implementation details on Wireless Open-Access Research Platform (WARP) [14].

#### A. Node Locations

We used five nodes, labeled as nodes Na, Nb, Nc, Nd, and Ne. The nodes were placed at locations shown in Fig. 2. Nodes Na, Nb, Nc, Nd, and Ne were located at a height of 1.5, 1.5, 1.4, 1.7, and 2.0 m, respectively, above the floor. Experiments were conducted in the second floor of a three-floor office building and were performed both at night and during office work hours with people walking in and out of the rooms. The five-node setup allowed us to evaluate ten different two-node links. The ten link pairs, their internode distance, and the type of channel for each link are shown in Table II. Our choices allowed us to create line-of-sight channels and also extremely challenging multiwall propagation environments, which represented a typical WiFi deployment. In contrast, the experiment setup in [11] was located at least 20 m from the nearest wall, which does not capture some typical WiFi scenarios. For experimental results in [5], [7], and [11], the distance between communicating nodes was not reported.

TABLE III  
NUMBER OF ANTENNAS AND RADIOS PER NODE USED BY THE DIFFERENT FD AND HD SYSTEMS THAT WERE EVALUATED VIA EXPERIMENTS

System	Number of antennas per node	Number of up-converting radio chains per node	Number of down-converting radio chains per node	Total number of radio chains per node
FD $2 \times 1$	3	3	1	4
HD $3 \times 1$	3	3	1	4
HD $2 \times 2$	2	2	2	4
FD $1 \times 1$	2	2	1	3
HD $2 \times 1$	2	2	1	3

### B. FD and HD Modes

For each of the ten links, we ran experiments for the following physical layers: FD  $1 \times 1$  (FD1  $\times 1$ ), FD  $2 \times 1$  (FD2  $\times 1$ ), HD  $2 \times 1$  (HD2  $\times 1$ ), HD  $3 \times 1$  (HD3  $\times 1$ ), and HD  $2 \times 2$  (HD2  $\times 2$ ). Experimental results obtained for the five systems have the necessary data to evaluate the performance of our FD design and compare its performance with HD systems, which use the same or less radio resources per node. Note that an HD  $M \times N$  node needs  $M$  upconverting radio chains and  $N$  downconverting radio chains for a total of  $M + N$  radio chains. In contrast, our proposed FD  $M' \times N'$  node uses  $M'$  upconverting radio chains for transmission,  $N'$  downconverting radio chains, and  $N'$  upconverting radio chains for self-interference cancelation for a total  $M' + 2N'$  radio chains per node for any  $M', N' \geq 1$ . For all five PHY configurations listed, the total number of chains is no more than four. That is,  $M + N \leq 4$  for HD systems and  $M' + 2N' \leq 4$  for FD systems. Table III shows the number of radios and antennas per node used by each of the FD and HD systems considered. We will compare the performance of FD and HD systems, which use the same number of radios per node. The performance of FD2  $\times 1$  will be compared with the performance of HD3  $\times 1$  and HD2  $\times 2$  systems. The performance of FD1  $\times 1$  will be compared with the performance of HD2  $\times 1$ .

For the experiments with more than one transmitter antenna, the multiple-antenna codes used were the following. For the FD2  $\times 1$  experiments, we used an Alamouti code [15]. Hence, in Fig. 1, the signals  $x_{i,1}$  and  $x_{i,2}$  correspond to Alamouti encoded symbols. The HD2  $\times 1$  experiments also used an Alamouti code. The HD3  $\times 1$  experiments used a rate 3/4 orthogonal space-time block code (OSTBC) from MATLAB MIMO library [16]. The HD2  $\times 2$  experiments used spatial multiplexing for two spatial streams, and receive processing was implemented using channel inversion.

We note that an FD2  $\times 1$  Alamouti implementation using our proposed wideband MIMO canceler requires three antennas per node, which is less than what is required by the MIMO cancelation techniques proposed in [11]. The MIMO antenna cancelation technique in [11] would require at least four antennas per node. The transmitter/receiver antenna cancelation technique proposed in [11] requires six antennas per node for the implementation of an FD2  $\times 1$  Alamouti system.

### C. Multiantenna Placements

We considered two possible antenna placements for the FD and HD experiments. For each antenna placement, we considered two cases, i.e., antennas with a device (a 15-in MacBook

Pro laptop) and without a device. Hence, we considered a total of four different configurations, as shown in Table I. For all the configurations, R1 was used as the receive antenna for all the systems that used only one receiver antenna, i.e., FD1  $\times 1$ , FD2  $\times 1$ , HD2  $\times 1$ , and HD3  $\times 1$ . For HD2  $\times 2$ , all the configurations used R1 and R2 as receiver antennas. For all the configurations and systems evaluated, if  $M$  antennas were required for transmission, we used antennas T1 to  $TM$ .

The antennas used in experiments [17] are designed for 2.4-GHz operation, with vertical polarization, and have a toroid-like radiation pattern shown in [17]. In A1, the FD experiments correspond to the case where the main lobe of the receiver antenna (R1) is in the same direction as the main lobe of T1 and orthogonal to the main lobe of T2. In A2, the FD experiments correspond to the case where the receiver (R1) main lobe is orthogonal to the main lobe of both T1 and T2. As experiments will demonstrate, the orthogonal placement of the transmitter and receiver main lobes in A2 will help reduce self-interference. Hence, A2 will result in larger PS than A1. Experimental results in Section IV will also demonstrate and quantify the increase in PS achieved by placing antennas appropriately around a device.

### D. Transmit Power Normalization

For a fair comparison between FD and HD systems, the total energy transmitted by an FD node must be the same as the total energy transmitted by an HD node. Since energy is power times transmission time, equation  $P_i^{\text{FD}} T_i^{\text{FD}} = P_i^{\text{HD}} T_i^{\text{HD}}$  defines the relationship between FD and HD power values, where  $P_i^{\text{FD}}$  denotes the transmission power use by node  $i$  in FD mode,  $P_i^{\text{HD}}$  denotes the transmission power used by node  $i$  in HD mode,  $T_i^{\text{FD}}$  denotes the duration of a transmission from node  $i$  in FD mode, and  $T_i^{\text{HD}}$  denotes the duration of a transmission from node  $i$  in HD mode.

Consider finite duration  $\tau$  of time for bidirectional communication between nodes 1 and 2. From time constraints for FD and HD, we have  $T_1^{\text{FD}} = T_2^{\text{FD}} = \tau$  and  $T_1^{\text{HD}} + T_2^{\text{HD}} = \tau$ . We define  $\beta = T_1^{\text{HD}}/\tau$ . Using the definition of  $\beta$  and the time constraints, we obtain that, for a fair comparison between FD and HD systems, the node power values used in FD and HD must satisfy  $P_1^{\text{FD}} = P_1^{\text{HD}} \beta$  and  $P_2^{\text{FD}} = P_2^{\text{HD}} (1 - \beta)$ .

Notice that this power allocation does not impose any constraint on the maximum power assigned to a node. However, in real systems, the maximum instantaneous radiated power is limited and is typically defined in standards. Hence, to include practical considerations in our power assignment equations, we define  $\Pi$  as the maximum power that can be radiated by the

network (not just one node, but all the nodes in the network together) at any time. Since HD transmissions from each node are orthogonal in time, it implies that in a network with two nodes  $i = 1, 2$ , the transmission power values must be such that  $P_1^{\text{HD}} \leq \Pi$  and  $P_2^{\text{HD}} \leq \Pi$ . In contrast, since FD transmissions from each node are simultaneous, the instantaneous radiated power constraint of  $\Pi$  translates to a power constraint of  $P_1^{\text{FD}} + P_2^{\text{FD}} \leq \Pi$  for FD nodes. Thus, we ensure that at any given time, a network with FD nodes radiates the same power that would be radiated by a network with HD nodes. We note that our power normalization handicaps the FD by using less power compared with HD and thus can be considered as lower bounds to the improvements offered by FD.

All our experiments correspond to an instantaneous power constraint of  $\Pi = 8$  dBm, and we achieve this constraint with equality. Hence, our experiments correspond to the following transmit power assignments:  $P_1^{\text{HD}} = P_2^{\text{HD}} = 8$  dBm,  $P_1^{\text{FD}} = 8$  dBm +  $10 \log_{10}(\beta)$ , and  $P_2^{\text{FD}} = 8$  dBm +  $10 \log_{10}(1 - \beta)$ . We performed only symmetric experiments, where  $\beta = 0.5$ , leading to  $P_1^{\text{FD}} = P_2^{\text{FD}} = 5$  dBm. We note that our experiments use multiple links with different internode placements and propagation environments, giving rise to different received SNR data points with the same transmit power values.

The radios used in our experiments can transmit at a maximum power value of 25 dBm. However, we observed that the radio's transmitter power versus gain setting relation is linear only for output power values between 0 and 15 dBm for OFDM signals of 20-MHz bandwidth used in our experiments. Consequently, for our experiments, we chose transmission power values that lie close to the middle of the linear range of the transmitter radios. Accounting for amplifier nonlinearities and their impact on cancelation coefficients  $b_{i,m,n}$  will be the focus of future work.

#### E. WARP Implementation and Testbed Setup

Digital and analog signal processing at a node were implemented using the WARPLab framework [14]. The WARPLab framework facilitates experiment implementation by allowing the use of MATLAB for digital signal processing and the use of WARP [14] hardware for real-time over-the-air transmission and reception.

All FD and HD experiments were conducted at a 2.4-GHz WiFi channel without any other concurrent traffic. In all our experiments, the nodes shared the same carrier frequency reference clock. All systems implemented have a bandwidth of 20 MHz using 64 subcarriers with 48 subcarriers used for payload as specified in one of the possible WiFi modes [26].

For each of the ten links considered, we ran experiments with both nodes using the same antenna/device configuration, and we considered all the possible combinations for the ten different links and four possible configurations shown in Table I. Thus, there were a total of 40 different scenarios. For each scenario in the FD/HD system considered, an experiment consisted of transmitting 90 packets from each of the nodes in the link. Each packet transmitted consisted of 68 OFDM symbols (the number of OFDM symbols per packet was limited by buffer sizes in the WARPLab framework), and each subcarrier was modulated

using QPSK. Since there were 48 payload subcarriers per OFDM symbol, the total number of bits transmitted per packet per node was equal to 6528 and the total number of bits transmitted per node in 90 packets was equal to 587 520.

#### IV. PHYSICAL LAYER EVALUATION: CANCELER PERFORMANCE

Here, we characterize the performance of the self-interference cancelation stages. We demonstrate that our FD design can achieve self-interference cancelation values, which can be larger than what has been reported in prior work.

##### A. Metric for Canceler Analysis

We measured the self-interference power after each stage of cancelation for each packet transmitted by a node in FD mode. For each stage of cancelation, the amount of cancelation (in decibels) was computed as the difference between the self-interference power before cancelation and the self-interference power after cancelation. The measurement of the self-interference power after each cancelation stage was computed based on the received signal strength indicator (RSSI) reading provided by the WARP radios. A more detailed explanation of the power measurements is provided in [18].

##### B. Performance of PS

*Result 1 (Gain from Antenna Placement and Orientation):* The amount of PS increases by as much as 15 dB for the placement where: 1) the receiver antenna is placed orthogonal to the transmitter antennas responsible for self-interference; and (b) the device-induced path loss is increased.

Fig. 3(a) shows a characterization of the amount of PS achieved by the four different configurations listed in Table I. First, we observe that at a cumulative distribution function (CDF) value of 0.5, configuration A1 with device achieves approximately 10 dB better cancelation than A1 without device. Similarly, configuration A2 with device achieves approximately 10 dB better cancelation than A2 without device. Hence, we conclude that placing antennas around a device improves the PS by approximately 10 dB.

Second, we observe that at a CDF value of 0.5, configuration A2 with device achieves approximately 5 dB better cancelation than A1 with device. Similarly, A2 without device achieves approximately 5 dB better cancelation than A1 without device. Hence, we conclude that A2 improves the PS by approximately 5 dB with respect to A1. This improvement is due to the fact that, in A2, the receiver antenna main lobe is placed orthogonal with respect to the transmitter antennas' main lobe. Consequently, A2 results in less coupling between self-interfering antennas, and this results in larger levels of PS.

Recent characterizations of PS mechanisms [5], [6] demonstrate levels of PS lower than 60 dB. Our results in Fig. 3(a) show that taking into account the antenna pattern and placing the antennas around the FD device serve as further means of PS and help achieve PS values between 60 and 70 dB. Comparing the cancelation values for A1 without device and A2 with device in Fig. 3(a), we observe that through-device cancelation



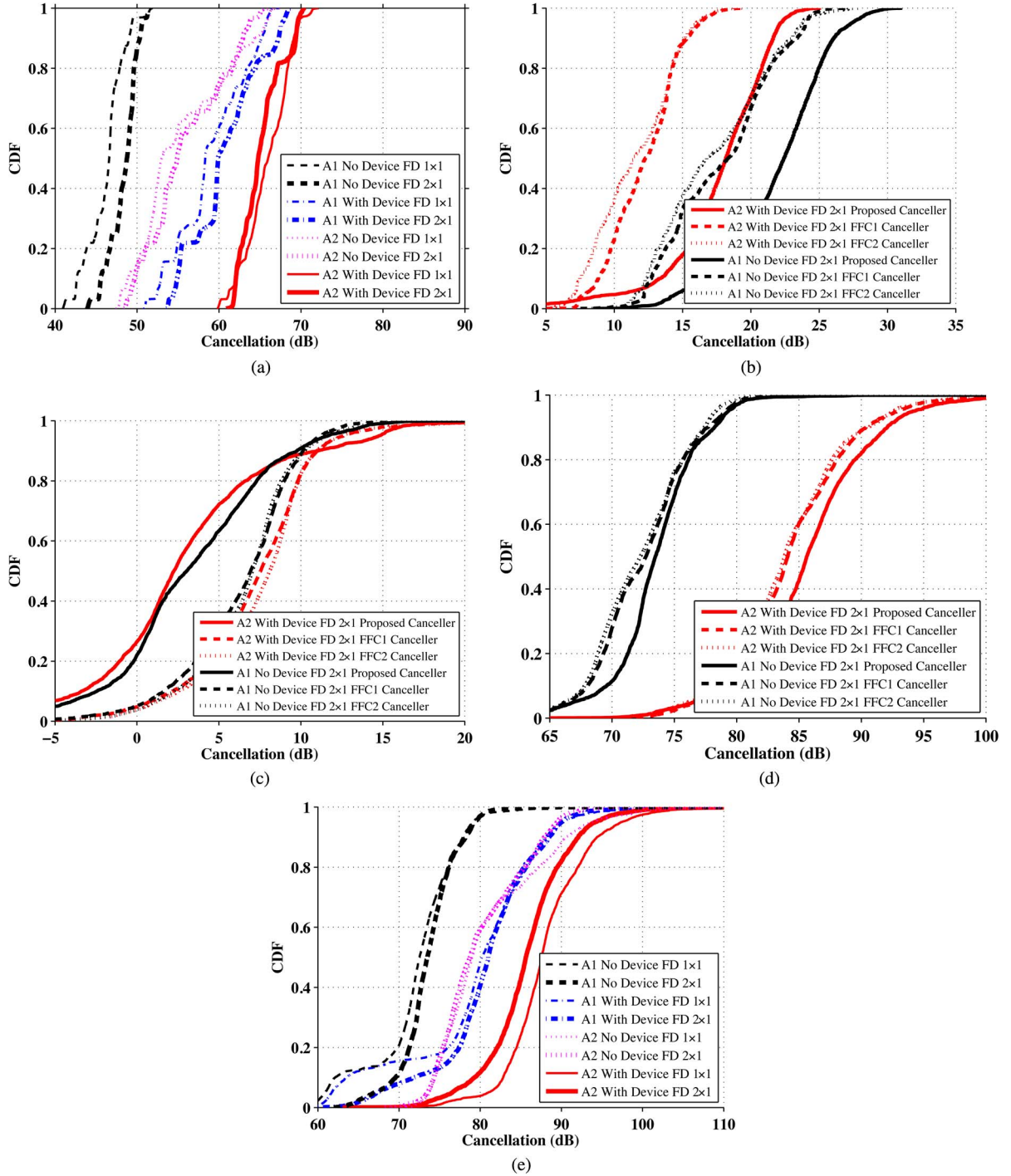


Fig. 3. CDF of the amount of cancellation for different cancelers and different antenna placements. (a) Passive cancellation for four different antenna placements. (b) AC for different analog cancelers. The results are shown for two different placements. (c) DC when the same digital canceler is applied after different analog cancelers. The results are shown for two different placements. (d) Total cancellation for systems that have the same PS and DC mechanisms but different analog cancelers. The results are shown for two different placements. (e) Total cancellation for different antenna placements and using our proposed per subcarrier analog canceler and digital canceler.

and orthogonal antenna placement improve the amount of PS by approximately 15 dB.

**Result 2 (Impact of PS on Self-Interference Channel):** As the amount of PS increases, the wireless self-interference channel becomes more frequency selective.

In our implementation of the analog canceler, we compute the cancellation coefficient per subcarrier  $b_{i,m,n}[k]$ , as shown in (1). Hence,  $b_{i,m,n}[k]$  is the ratio of the estimate of the

self-interference wireless channel  $\hat{h}_{i,m,n}[k]$  and the wire channel  $\hat{h}_{i,n}^W[k]$ . Since the wire channel  $\hat{h}_{i,n}^W[k]$  is frequency flat, variations of the cancellation coefficient  $b_{i,m,n}[k]$  as a function of the subcarrier index are due to variations of the self-interference channel  $\mathbf{h}_{i,m,n}$  as a function of frequency. If  $\mathbf{h}_{i,m,n}$  is frequency flat, then  $b_{i,m,n}[k]$  will be the same across all subcarriers, else  $b_{i,m,n}[k]$  will vary for different subcarriers if  $\mathbf{h}_{i,m,n}$  is frequency selective.

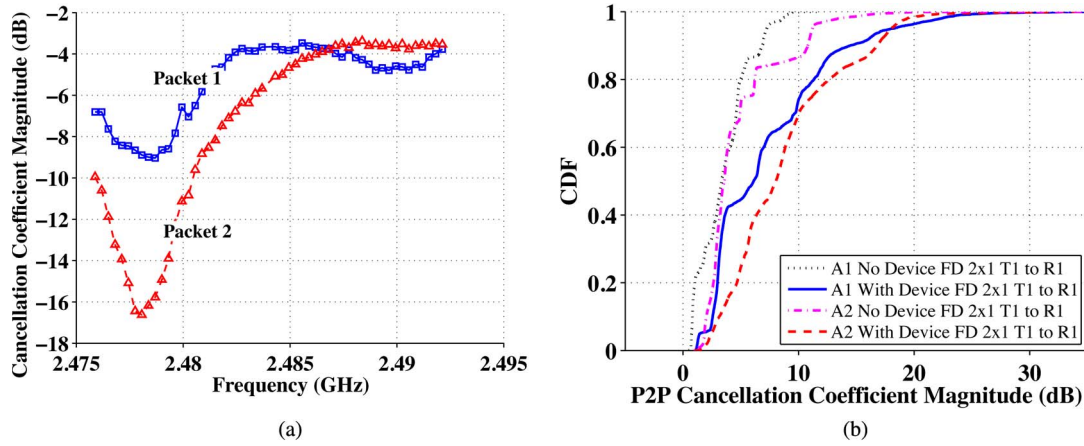


Fig. 4. Characterization of the effect of passive cancellation on the frequency response of the self-interference channel. (a) Cancellation coefficient per subcarrier captured for two subsequent packets. (b) CDF of the p2p value of the cancellation coefficient magnitude.

Fig. 4(a) shows the magnitude of the cancellation coefficients  $b_{i,m,n}[k]$  for each of the 48 data subcarriers captured for two subsequent packets. The subcarrier spacing is 0.3125 MHz as in 802.11 for a 20-MHz bandwidth channel. We observe that as a function of subcarriers, the channel attenuation can significantly vary across frequency, and thus, approximating self-interference channel as frequency flat can be highly inaccurate.

To completely characterize the statistical variations in self-interference channel across frequency, we use the measure of peak-to-peak (p2p) value of the magnitude of the cancellation coefficient  $|b_{i,m,n}|^{\text{p2p}}$ , as follows:

$$|b_{i,m,n}|^{\text{p2p}} = \frac{\max_{k \in \{1, \dots, K\}} |b_{i,m,n}[k]|^2}{\min_{k \in \{1, \dots, K\}} |b_{i,m,n}[k]|^2}. \quad (2)$$

If the self-interference channel  $\mathbf{h}_{i,m,n}$  is a flat-frequency channel, then  $|b_{i,m,n}|^{\text{p2p}} = 1$ , and for a frequency-selective channel,  $|b_{i,m,n}|^{\text{p2p}}$  will be larger than 1. For each FD2  $\times$  1 experiment, we computed the value of  $|b_{i,m,n}|^{\text{p2p}}$  between transmitter antenna 1 (T1) and receiver antenna 1 (R1). Fig. 4(b) shows a characterization of the cancellation coefficient for the four different antenna configurations listed in Table I. Fig. 4(b) shows that the channel can have large variations in magnitude in the practical case of antennas placed around a device, with a median of 9-dB p2p magnitude variations for A2 with device.

Comparing Fig. 4(b) with Fig. 3(a), we observe the following. The larger the PS, the larger the variations of the self-interference channel as a function of frequency. Intuitively, this makes sense since PS of the self-interference corresponds to suppression of the strongest line-of-sight paths between self-interfering antennas. As the line-of-sight path is weakened, the self-interference channel becomes more dependent on weaker reflected multipaths, and this results in larger frequency selectivity of the self-interference channel.

For scenarios where the channel is frequency selective, the active AC must be able to adapt to the frequency variations of the channel per subcarrier, as is the case in our proposed implementation of active AC.

### C. Performance of AC

To better illustrate the importance of the per subcarrier adaptation of the analog canceler, we compare the performance

of our per subcarrier AC with the performance of two AC schemes that do not adapt the magnitude of the cancellation coefficient per subcarrier and use the same magnitude of the cancellation coefficient for all subcarriers (as is the case for the analog canceler schemes considered in [4], [5], and [7]).

Specifically, we consider the following two flat-frequency cancelers.

- 1) Flat-frequency canceler 1 (FFC1): For this canceler, the magnitude of the cancellation coefficient is the same for all subcarriers and is computed as the average from the required per subcarrier as  $(1/K) \sum_{k=1}^K |b_{i,m,n}[k]|$ .
- 2) Flat-frequency canceler 2 (FFC2): For this canceler, the magnitude of the cancellation coefficient is the same for all subcarriers and is computed as the value required by the middle subcarrier in the band; hence, it is equal to  $|b_{i,m,n}[K/2]|$ .

We highlight that the three analog cancelers, i.e., per-subcarrier, FFC1, and FFC2, are different only in the magnitude of the cancellation coefficient but have the same per-subcarrier adaptation of the phase of the cancellation coefficient. The previous simplification made our implementation easier for comparison while still allowing us to demonstrate the importance of per subcarrier adaptation.

Fig. 3(b) shows the amount of active AC that our proposed AC achieves for configurations A1 without device and A2 with device, and it also shows the performance of FFC1 and FFC2. We observe that per-subcarrier adaptation of the magnitude of the cancellation coefficient achieves larger AC than FFC1 and FFC2. In Fig. 3(b), we approximate that per-subcarrier adaptation of the magnitude of the cancellation coefficient achieves approximately 5 dB larger cancellation than FFC1 and FFC2. Hence, we obtain the following result.

**Result 3 (Gains From Per-Subcarrier Cancellation):** Per-subcarrier AC improves the amount of AC by approximately 5 dB, as compared with cancelers that do not adjust the magnitude of the cancellation coefficient per subcarrier.

In Fig. 3(b), we observe that the AC was larger for the configuration without device compared with the configuration with device. Hence, the roles for best/worst cancellation are inverted with respect to what we had observed in Fig. 3(a), where configurations with device showed better performance



than configurations without device. The reason the configuration with device achieves lower levels of AC is because AC is based on an estimate of the self-interference channel. The weaker the received self-interference (self-interference at the receiver antenna), the worse the estimate of the self-interfering channel and the worse the amount of cancellation achieved [18]–[20]. Configurations with device have the weakest levels of received self-interference because they achieve the largest PS.

#### D. Performance of DC

We are now interested in characterizing the performance of DC. For this purpose, we quantify the amount of DC achieved when placing a digital canceler after each of the three analog cancelers analyzed in Fig. 3(b). These results for DC are shown in Fig. 3(c). We observe that, when DC is placed after AC, the amount of DC achieved after our proposed per subcarrier analog canceler is less than the amount of DC achieved after FFC1 and FFC2 cancelers. The reason for this behavior is that, as the amount of AC increases, the residual self-interference decreases; hence, there is more noise in the estimation of the residual self-interference after AC, and this results in less DC. In the limit, if AC can achieve infinite decibels of cancellation (perfect cancellation), then DC becomes unnecessary and applying DC in this limit case will only lead to an increase in the noise [18]–[20].

#### E. Total Cancellation of Physical Layer Design

We now compare the results for total cancellation for systems that have the same PS and DC mechanisms but use different analog cancelers. The different analog cancelers are those analyzed in Fig. 3(b) (i.e., per-subcarrier, FFC1, and FFC2). The results for total cancellation are shown in Fig. 3(d). We observe that using our proposed per-subcarrier AC achieves the largest total cancellation and the improvement is approximately 3 dB. We note that the advantage of per-subcarrier AC is not only that it improves the total cancellation by 3 dB but also that it achieves larger pre-ADC cancellation compared with the FFC1 and FFC2 systems. Predictably, we will show in Section V-B larger per-subcarrier AC results in higher rates than using FFC1 or FFC2 cancelers.

Next, we analyze the total cancellation of our design for the four different antenna configurations showed in Table I; the results are shown in Fig. 3(e). We observe that A2 with device achieves the largest total cancellation with cancellation values between 70 and 100 dB, with a median of 85-dB cancellation. In general, we observe that, for the same implementation of active AC and DC, the largest cancellation will be obtained with the configuration that achieves the largest PS. This leads to an important direction that *antenna design and placement* are crucial to achieve practical FD, and the design has to be cognizant of the device dimensions and placement. Finally, we observe that the performance of the cancellation scheme was very similar between the  $FD2 \times 1$  and  $FD1 \times 1$  systems.

To the best of our knowledge, the levels of cancellation achieved by our A2 with device implementation are the best reported for a wideband 20-MHz multiple-subcarrier and

multiple-antenna FD system. The results provided in [5], [6], [10], [11], and [20] correspond to narrow-band systems. The results in [7] are for a multiple-subcarrier system with 10-MHz bandwidth and correspond to a single interference antenna. The work in [7], [10], and [11] does not report a measured value of total cancellation for a combination of passive, active AC, and active DC and focuses only on characterizing a subset of these types of cancelations. Finally, none of the previous works [5]–[7], [10], [11], [20] report cancelations larger than 73 dB. Hence, we have the following result.

*Result 4:* Our proposed self-interference canceler design, for 20-MHz  $FD1 \times 1$  and  $FD2 \times 1$  systems, achieves total self-interference cancellation values similar or larger than what prior work has reported.

Even with high number for interference cancellation, the self-interference is not reduced to the noise floor. However, as we will show in Section V-B, there are conditions under which our FD implementation can achieve higher rates than HD in WiFi SNR ranges.

### V. PHYSICAL LAYER EVALUATION: RATE PERFORMANCE

#### A. Metric for PHY Rate Analysis: Empirical ERs

The ER is the fundamental measure of PHY layer capacity in fading channels [21] and is an upper bound on the throughput that would be achieved by any MAC protocol. The ERs become the starting point for a system designer to choose actual constellation sizes and code rates. The ER for transmission to node  $i$  is given by  $\mathbb{E}(R_i) = \mathbb{E}[\log \det(I + H[p]QH[p]^\dagger)]$ , where the expected value is computed as the average over all the packets  $p$  transmitted to node  $i$ ,  $H[p]$  is the channel matrix between node  $i$  and the transmitter, and  $Q$  is the input covariance matrix [21].

The empirical ER for SISO case in experiments is computed based on an estimate of  $SINR_i[p]$ , which is the postprocessing signal-to-self-interference-plus-noise ratio for packet  $p$  received at node  $i$ . We estimate  $SINR_i[p]$  from transmitted and received constellation symbols as follows. Constellation symbol  $s_i$  is sent to node  $i$  via the wireless channel. Node  $i$  processes the received signal and computes  $\hat{s}_i = H^{-1}[p]y[p]$  (where  $y[p]$  is the received signal), which is the estimate of  $s_i$ . The average energy of the error or noise is given by  $\mathbb{E}[|s_i - \hat{s}_i|^2]$ . Postprocessing SINR for packet  $p$  received at node  $i$ , i.e.,  $SINR_i[p]$ , is computed as  $SINR_i[p] = (\mathbb{E}[|s_i|^2]) / (\mathbb{E}[|s_i - \hat{s}_i|^2])$  where the expected value is computed as the average over all the symbols transmitted to node  $i$  during packet  $p$ . For the  $2 \times 1$  and  $3 \times 1$  MISO systems, we estimate  $\hat{s}_i$  using the corresponding space-time block code combining (for example, Alamouti combining for  $2 \times 1$ ). For the case of two transmit and two receive antennas, we find the estimate of the transmit signal as  $H^{-1}y$  and then find the  $SINR_i[p]$  for all the streams. The empirical ER is the sum of  $\mathbb{E}[\log(1 + SINR[p])]$  over each stream.

In this paper, we will also use preprocessing SNR, which is defined as follows. In our experiments, we found the estimate of average noise power to be  $-90$  dBm for all experiments. This estimate of noise power was based on the radio data sheet and on node calibration performed before the experiments

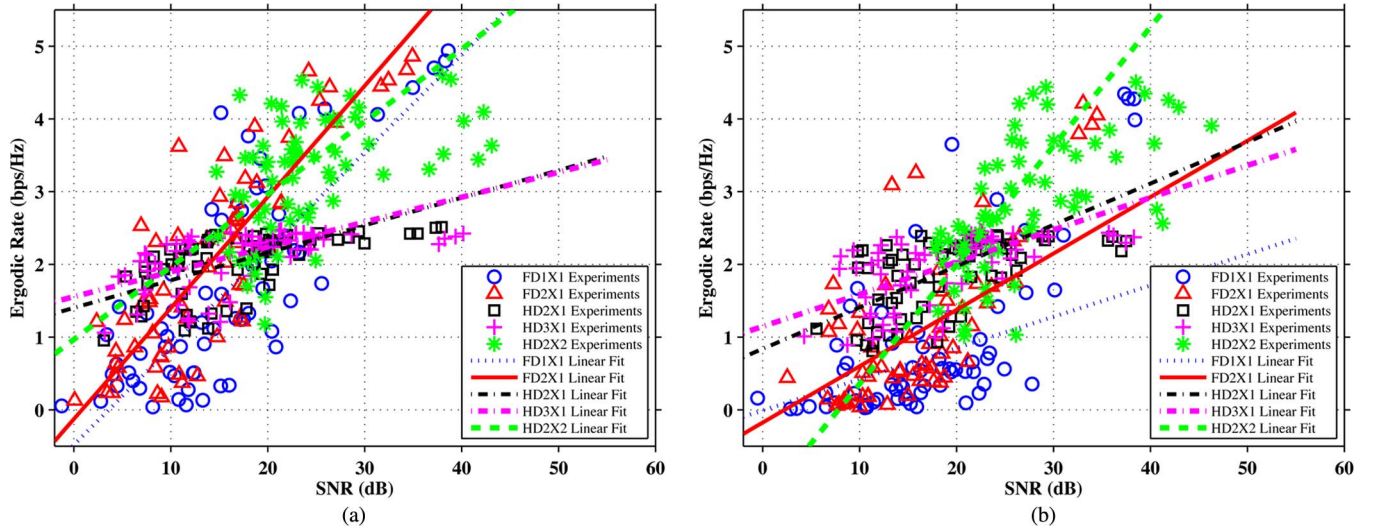


Fig. 5. ER as a function of the preprocessing SNR and linear fit approximations. (a) Results for antennas placed around the device (device in the middle). (b) Results for antennas without device in the middle.

were conducted. Then, the preprocessing SNR is defined as  $\text{SNR}(\text{dB}) = \text{RSSI}(\text{dBm}) - N_0(\text{dBm})$ . In our experiments, we estimate  $N_0 = -90$  dBm. Furthermore, we will also use SNR to denote preprocessing SNR.

Since the two-way communication in HD is achieved by time sharing the link with a fraction of time  $\beta$  dedicated for transmission from node 1 and a fraction of time  $1 - \beta$  dedicated for transmission from node 2, the ER for each node in an HD two-node communication system has to be scaled by their time of transmission, leading to  $\mathbb{E}(R_1^{\text{HD}}) = \beta \mathbb{E}(R_1)$  and  $\mathbb{E}(R_2^{\text{HD}}) = (1 - \beta) \mathbb{E}(R_2)$ . We performed only symmetric experiments where  $\beta = 0.5$ . For FD transmissions, since both nodes transmit at the same time, the ER for each node in an FD communication system is given by  $\mathbb{E}(R_1^{\text{FD}}) = \mathbb{E}(R_1)$  and  $\mathbb{E}(R_2^{\text{FD}}) = \mathbb{E}(R_2)$ .

### B. Comparison of FD and HD ERs

Previous work on FD implementation [5], [7], [11] had not considered the case of placing antennas around the FD device. In Section IV, we demonstrated that placing the interfering antennas around the FD device can improve the total cancellation. Here, we show that this increase in total cancellation results in FD rate gains at WiFi ranges.

Experimental results in Fig. 5 show the ER for transmission to a node in a two-way link as a function of the preprocessing SNR. Experimental results in Fig. 5(a) correspond to the case of antennas placed around the device (configurations A1 and A2 with device in Table I). Experimental results in Fig. 5(b) correspond to the case of antennas placed without the device in the middle (configurations A1 and A2 without device in Table I). For each FD/HD system and antenna configuration, we ran two experiments for links 1, 6, 7, 8, 9, and 10, and we ran one experiment for links 2, 3, 4, and 5. Hence, for each FD/HD system and antenna configuration, we ran 16 experiments (an experiment consisted in transmitting 90 packets from each of the two nodes in the link). Results in Fig. 5 are per node per link per experiment per system. Hence, Fig. 5(a) shows 64 markers for each system, which corresponds to two an-

tenna configurations (i.e., A1 without device and A2 without device)  $\times$  16 experiments  $\times$  2 nodes. Similarly, Fig. 5(b) shows 64 markers for each system.

For each system depicted in Fig. 5, we present experimental results with markers and also show a line that corresponds to a linear fit of the experimental results. These results show the increase in ER with preprocessing SNR. To compute the expected values in the preprocessing SNR and the postprocessing SINR, we averaged the corresponding power measurements per packet over the 90 packets received during an experiment run. The linear fit for the FD2  $\times$  1, FD1  $\times$  1, and HD2  $\times$  2 systems was computed based on the data points that lay between 5- and 30-dB SNRs. We only used this interval for the fit because most of the data points lie inside this interval and because this interval contains SNR values typical of WiFi operation ( $\text{SNR} \leq 30$  dB). For the HD2  $\times$  1 and HD3  $\times$  1 systems, the linear fit was computed based on the data points that lay between 5 and 23 dB. The reason we used this interval for the HD2  $\times$  1 and HD3  $\times$  1 linear fits is because we observe that, for SNR values above 23 dB, the rate of HD2  $\times$  1 and HD3  $\times$  1 systems does not increase as the SNR increases. The observed performance ceiling can be explained as follows. The postprocessing SINR cannot be arbitrarily increased due to the error floor caused by quantization, imperfect channel estimation, and other hardware limitations. Hence, even if preprocessing SNR is increased, beyond certain point, postprocessing SINR does not increase accordingly. Different schemes postprocess the received signal differently and thus will hit a performance ceiling at different preprocessing SNRs. Since HD 2  $\times$  1 and 3  $\times$  1 implementations use OSTBC and perform coherent combining, the postprocessing SINR reaches the performance ceiling faster than HD 2  $\times$  2 and FD 2  $\times$  2 implementations. In our experiments, we observed that HD 2  $\times$  1 and HD 3  $\times$  1 implementations reach a performance ceiling at preprocessing SNR  $\approx 23$  dB. We have observed that the performance ceiling of our implementation is a function of the bandwidth. When we use only one subcarrier (625-kHz-bandwidth system), we do not observe a performance ceiling. Furthermore, our FD and HD 2  $\times$  2 implementations did not reach a performance

ceiling until the maximum SNR (around 40 dB) used in the experiments.

We now analyze the rate performance of FD and HD systems that do not use antenna placement around the device. In Fig. 5(b), we observe that for  $\text{SNR} \leq 30$  dB, the experiment data points for the FD systems are mostly below the experiment data points for HD systems. Consequently, since the linear fits only consider experiment data points for which the SNR was lower than 30 dB, the linear fit for the  $\text{FD2} \times 1$  and  $\text{FD1} \times 1$  systems lies below the linear fit for the HD systems. The experimental data points in Fig. 5(b) show that  $\text{FD2} \times 1$  and  $\text{FD1} \times 1$  systems can have similar or large rates than HD systems at SNR values larger than 30 dB. However, SNR values larger than 30 dB are not typical in WiFi systems. Consequently, from the results in Fig. 5(b), we conclude that FD gains at WiFi ranges cannot be achieved with self-interference cancelation schemes that have a median cancelation of 78 dB or less, as is the case for the FD systems without device considered in our experiments.

We next analyze the performance of FD and HD systems that use antenna placement around the device. By comparing the experimental data and linear fits in Fig. 5(a) with the experimental data and linear fits in Fig. 5(b), we observe the following. Placing antennas around the device (device in the middle) improves the performance of FD and HD systems with respect to the case where antennas are not placed around the device. In other words, for the same SNR, FD and HD rates tend to be higher when the antennas are placed around the device. For the HD systems, this is explained by the fact that placing antennas around the device reduces the transmitter and receiver correlations, and as these correlations decrease, the HD rates increase [21], [22]. For the FD systems, this is explained by the fact that placing the antennas around the device achieves larger cancelation than the configuration without a device in the middle of the antennas.

The larger self-interference cancelation achieved by placing the antennas around the device yields the following result.

**Result 5:**  $\text{FD1} \times 1$  and  $\text{FD2} \times 1$  systems with antenna placement around the device can consistently achieve larger rates than  $\text{HD2} \times 2$ ,  $\text{HD3} \times 1$ , and  $\text{HD2} \times 1$  systems for the SNR range of 20–30 dB, thereby covering nearly half the range of a typical WiFi system.

Result 5 can be verified from Fig. 5(a). The linear fit for  $\text{FD2} \times 1$  and the linear fit for  $\text{HD2} \times 2$  in Fig. 5(a) show that  $\text{FD2} \times 1$  can achieve rates larger than  $\text{HD2} \times 2$  for SNRs approximately higher than 20 dB. Similarly, the linear fit for  $\text{FD1} \times 1$  and the linear fit for  $\text{HD3} \times 1$  in Fig. 5(a) show that  $\text{FD1} \times 1$  can achieve larger rates than  $\text{HD3} \times 1$  for SNRs approximately higher than 20 dB.

In Fig. 5(a), we note that, for the case where antennas are placed around a device, the FD systems have a larger multiplexing gain than all HD systems, where multiplexing gains are the slopes<sup>1</sup> of the rate–SNR curves in Fig. 5. For the case of

antennas without a device, in Fig. 5(b), we observe that most of the FD rates lie below 1.5 b/s/Hz, which explains the lower slopes of FD systems compared with HD systems when the antennas are placed without a device in the middle and when we consider SNRs lower than 30 dB for the linear fit. Thus, we obtain the following result.

**Result 6:**  $\text{FD1} \times 1$  and  $\text{FD2} \times 1$  systems were measured to have a larger multiplexing gain per node than  $\text{HD2} \times 2$ ,  $\text{HD3} \times 1$ , and  $\text{HD2} \times 1$  systems for the case where the antennas are placed around the device (device in the middle).

In Fig. 5(a), the slope of the fit for the  $\text{FD1} \times 1$  system is approximately 1.3 times larger than the slope of the fit for the  $\text{HD2} \times 2$  system and approximately 3.7 times larger than the slope of the fit for the  $\text{HD3} \times 1$  and  $\text{HD2} \times 1$  systems. The slope of the fit for the  $\text{FD2} \times 1$  system is approximately 1.5 times larger than the slopes of the fit for the  $\text{HD2} \times 2$  system and approximately 4.2 times larger than the slopes of the fit for the  $\text{HD3} \times 1$  and  $\text{HD2} \times 1$  systems.

$\text{FD1} \times 1$  and  $\text{FD2} \times 1$  systems have a larger slope than  $\text{HD3} \times 1$  and  $\text{HD2} \times 1$  systems because of the following reason. At high SNR, the  $\text{HD3} \times 1$  and  $\text{HD2} \times 1$  systems can have a maximum multiplexing gain per node of 0.5 since each node only transmits half the time. In contrast, at high SNR, the FD systems can have a maximum multiplexing gain per node of 1, which is not scaled by 0.5 since FD systems can transmit during the entire time slot. Thus, we conclude that  $\text{FD1} \times 1$  and  $\text{FD2} \times 1$  systems are expected to have steeper slopes for rate increase versus SNR compared with  $\text{HD2} \times 1$  and  $\text{HD3} \times 1$  systems. We think that a reason the fit for the FD systems achieves more than twice the slope of  $\text{HD3} \times 1$  and  $\text{HD2} \times 1$  systems is due to the performance ceiling of our implementation of  $\text{HD3} \times 1$  and  $\text{HD2} \times 1$ , which was explained earlier.

As evident from the results in Fig. 5(a),  $\text{FD1} \times 1$  and  $\text{FD2} \times 1$  rates can also have a larger slope than an  $\text{HD2} \times 2$  system, which is a little surprising but we conjecture the following reason. As previously discussed, the FD systems can have a maximum multiplexing gain of 1. At high SNR, a  $2 \times 2$  MIMO system can have a maximum system multiplexing gain of 2, which implies that  $\text{HD2} \times 2$  can have a maximum multiplexing gain per node of 1 (since each node transmits only half the time). As shown in [22], for a  $2 \times 2$  system to achieve maximum multiplexing gain, the mean channel condition number should be approximately 3.5 dB or less (see [22], where values of  $\rho_T = \rho_R = 0$  lead to a multiplexing gain of 2 at high SNR, and from [22], we compute that  $\rho_T = \rho_R = 0$  corresponds to a condition number of 3.5 dB, computed as  $10 \log_{10} \sqrt{(4 - 0.65)/0.65}$ ). From both our results and the results in [22], it appears that indoor channels typically do not have condition numbers that meet the aforementioned criterion, therefore reducing achieved multiplexing gains of MIMO systems compared with theoretical maximum. Fig. 6 shows the CDF of the condition number measured per packet from our experiment measurements. In Fig. 6, we observe that the probability of having a condition number less than or equal to 3.5 dB is small (less than 10%)

Next, we comment on the importance of per-subcarrier cancelation. The lower active AC achieved by FFC1 and FFC2

<sup>1</sup>If a system has multiplexing gain of  $r$ , then at high SNR, the rate in bits per second per hertz can be approximated as  $r \log_2 \text{SNR}$  and the slope of increase, in a plot where the  $y$ -axis is in bits per second per hertz and the  $x$ -axis is in decibels, is equal to  $(r \log_2 \text{SNR}) / (10 * \log_{10} \text{SNR}) = 0.332r$ .



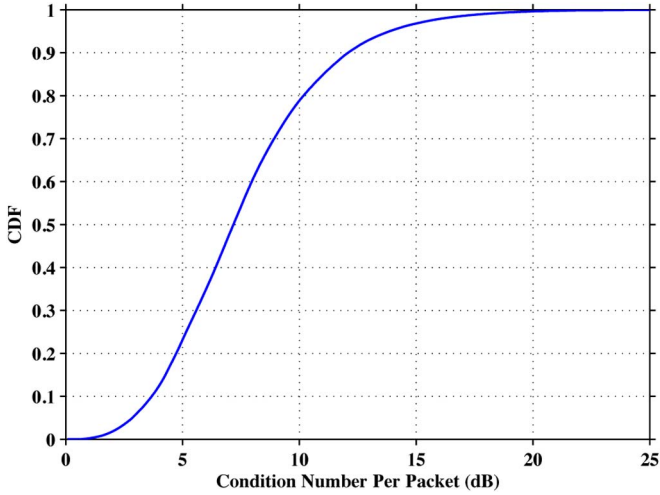


Fig. 6. CDF of condition number per packet computed from experiment measurements.

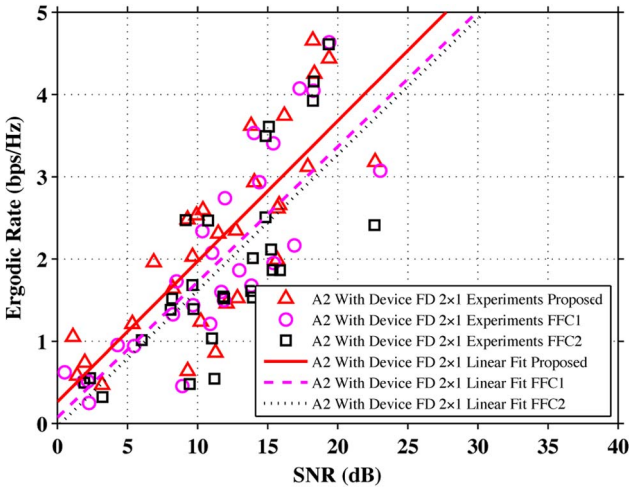


Fig. 7. ER versus preprocessing SNR performance for different analog cancelers.

in a frequency-selective environment [see Fig. 3(b)] results in degradation of the achievable rate performance, as shown in Fig. 7. For example, at an SNR of 15 dB, schemes FFC1 and FFC2 result in approximately 13% performance loss compared with our proposed scheme.

Finally, we note that, although through-device cancellation is a simple and effective means of cancellation, antenna placement techniques in [5], [10], and [11] may not be able to implement and take advantage of through-device cancellation. The reason is that antenna placement techniques in [5], [10], and [11] are designed under the assumption that the self-interference channel does not have multipath components. As we have shown in Section IV-B, placing the antennas around the device makes the multipath effect more severe. Consequently, the assumptions that should hold for antenna cancellations in [5], [10], and [11] to be effective may not hold (or hold for fewer realistic conditions) when the antennas are placed around a device.

## VI. MEDIA ACCESS CONTROL DESIGN

Here, we describe the design of the proposed MAC. The driving goal for FD MAC design is minimal changes to the current

WiFi standard to support both HD and FD nodes and, in the process, to accelerate its adoption. We limited our attention to support FD communication only between two nodes, i.e., when a mobile node and the AP have a packet for each other. With this in mind, we modified the standard HD 802.11 Distributed Coordination Function (DCF) MAC [23] [26] with RTS/CTS to add an FD mode. In the rest of this section, we describe the modifications to legacy WiFi MAC to support the FD mode, whereas the complete details are provided in [24].

We divide our discussion on the changes to legacy WiFi MAC in three parts: 1) discovery and transmission of FD packets; 2) management of ACKs; and 3) behavior of overhearing nodes.

*Discovery and Transmission of FD Packets:* The first challenge is to get an opportunistic FD data transmission between two nodes. This is achieved with the following changes from the existing standard 802.11 modules. We make use of the standard RTS and CTS packets. The sender (also known as the primary node) signals intent to send a data packet using an 802.11 RTS packet. The node receiving the RTS (secondary node) then discovers the transmit node id, which is needed to start the FD transfer to the sender. Since the secondary node knows that the primary sender will be transmitting, it finds opportunity to send FD data as follows.

In the standard 802.11 protocol, the RTS receiver sends a CTS frame and listens to the incoming data. However, in FD MAC, we would also like the secondary node to transmit to the primary immediately after sending the CTS frame [after the standard short interframe space (SIFS) time] whenever data are available. Note that at the head of the queue in the secondary node transmit buffer, there may not be a packet intended for the primary sender. We address this by making the secondary node inspect its queue and select the very first packet intended for the primary sender. If necessary, the secondary node further updates the network allocation vector (NAV) based on the original NAV it received during the RTS frame and the length of secondary packet.

In the standard 802.11 protocol, a node cannot receive a packet while transmitting. If there is such a simultaneous transmission (e.g., for RTS frames or for DATA frames if RTS/CTS is not used), there is no ACK (CTS for RTS or ACK for DATA) and the sender retransmits the packet. However, in our design, both transmission and reception of DATA and ACK frames can occur at the same time. Our FD MAC implementation checks if the received packet is from the other node involved in RTS-CTS exchange and accepts the packet if the NAV duration has not expired.

*Management of ACKs:* The second challenge for the two nodes involved in FD data transmission is to send and receive ACKs for the successful transmissions. In legacy 802.11, after sending the data, a node expects an ACK frame. However, in FD, since data are sent from both nodes simultaneously, each node gets data before it gets an ACK. This is fixed by accepting one data packet in the NAV duration and returning to the prior state where it is still waiting for ACK. However, reception of a second data transmission before reception of ACK would result in the node concluding that the data packets have collided.

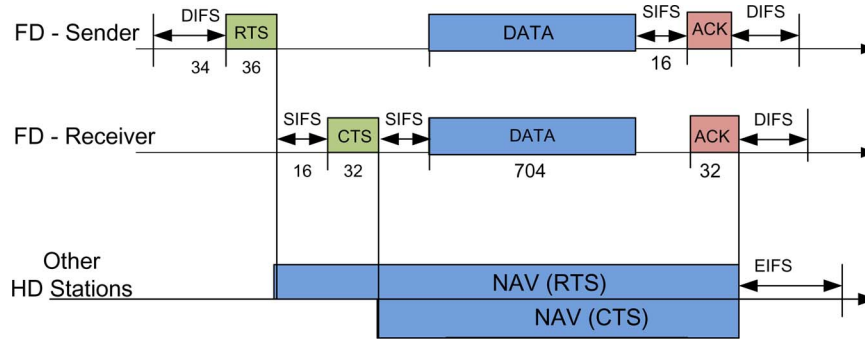


Fig. 8. FD MAC frames for 802.11a.

After the FD transmission, both the nodes involved in transmission are waiting for an ACK. In legacy 802.11, nodes cannot transmit while waiting for ACK until the ACK timeout duration has passed. This would lead to neither of the two nodes receiving ACK (since the other node will not transmit), thus leading to the ACK getting timed out at both nodes. To avoid this ACK timeout, FD MAC allows the nodes to send an ACK even while waiting for ACK from the other end. Furthermore, after sending the ACK, the node returns to the state where it is waiting for the ACK packet.

For asymmetric data packet lengths, the node sending a smaller length packet has to wait a long time to receive the ACK because the other node with larger packet length has not finished sending data. Thus, in FD MAC design, the wait time for the reception of the ACK packet for both nodes involved in the transmission is re-adjusted to the end of the NAV duration if necessary.

**Behavior of Overhearing Nodes:** The third challenge is to ensure that the node pair involved in FD communication does not get an unfair advantage of capturing the channel repeatedly. In the standard 802.11 model, all nodes use a longer wait time [extended interframe space (EIFS)] rather than the standard wait time [DCF interframe space (DIFS)] if they receive an erroneous packet, which is a packet for which the MAC header was not properly decoded or the PHY-RXEND.indication primitive has an error. The extended wait time is used to allow some other recipients for the packet who may have received the data correctly to be able to send an ACK frame in time. The need to use EIFS is reset if a packet is received correctly. In a system with FD nodes (either all FD or mixed FD and HD), all nodes that are not involved in FD transmission will detect an erroneous packet and thus wait for EIFS as per standard 802.11. However, the nodes involved in FD transmission do not find the reception erroneous and thus start their backoff timer after waiting for DIFS. Since the DIFS wait time is smaller than EIFS wait time, there is higher likelihood for one of the FD nodes to grab the channel again causing unfairness.

We propose two different strategies to solve this problem. The first is optimized for a system where all nodes are FD. In FD MAC design, FD nodes that receive a CTS packet successfully that is not intended for them ignore any erroneous packets during the NAV duration specified in CTS. Thus, the nodes will not subsequently detect an erroneous packet caused by collision of two data streams and therefore not switch to using the EIFS mode. Note that this change does not defeat

the purpose of EIFS since the NAV time has been already understood by the node, which includes the time taken for ACK transmission.

However, note that in a system with both FD and *legacy* HD stations, as shown in the timing diagram in Fig. 8, the HD nodes wait for EIFS rather than DIFS after an FD transmission between AP and an FD station in the system, leading to unfairness in the uplink throughput. To avoid unfairness, we propose a second strategy where FD nodes do not ignore erroneous receptions during NAV except for the two nodes involved in FD transmission to wait for EIFS after every FD message exchange. Furthermore, the two nodes involved in FD transmission use a waiting time of EIFS rather than DIFS after receiving ACK. The change in waiting time will lead to increased wait times when there are a lot of FD nodes while not compromising the uplink throughput of HD stations significantly. We will analyze both strategies in Section VII-D.

## VII. MEDIA ACCESS CONTROL EVALUATION

Here, we evaluate the FD MAC protocol discussed in Section VI using the commercial software package OPNET Modeler-Wireless [29]. We started with the standard 802.11 codebase available in OPNET and made the necessary modifications to implement FD MAC. Fig. 8 shows a typical FD framing structure where the RTS frame is followed by a SIFS time and a CTS frame. After another SIFS time, data transmission occurs simultaneously and is then followed by a SIFS and an ACK. The following timings in microseconds are shown from our evaluated 802.11a-based FD MAC implementation. For 18 Mb/s, DIFS = 34 μs, RTS = 36 μs, SIFS = 16 μs, CTS = 32 μs, Data = 704 μs, and ACK = 32 μs. Note that after an FD data transmission, the ACKs from both the nodes involved in the FD exchange are transmitted simultaneously.

For our MAC simulation results, we focus on the goodput, which we define as the effective throughput taking collisions, packet error, and retransmissions into account. First, we study how goodput varies with different modulation formats and varying packet sizes for a system with one AP and one FD node (STA). Next, we extend our understanding regarding goodput performance for a system with multiple FD nodes. Furthermore, we study a system with a mix of FD and HD nodes, where the HD nodes ignore collisions during the NAV duration set by an RTS/CTS; this is a nonstandard behavior for legacy HD nodes but serves to highlight the coexistence dynamics. Finally, we

TABLE IV  
MAC SIMULATION PARAMETER SET

Parameter	Value
# Nodes	2 (AP+1) to 9 (AP+8)
Transmit power	12 dBm
Center frequency	2400 MHz
Free space path loss	63 dB
RSSI	-51 dBm
Self-interf. cancellation	Default 85 dB
Modulation	QPSK, 18 Mbps
Data Asymmetry	5% to 100%
Packet size	40 to 1500 bytes uplink, 1500 bytes downlink
BER model	Q-function, treating self-interference as noise
Traffic model	Full buffer
AP Queue	Single queue
Buffer size	25600 KB
Simulation time	10 sec

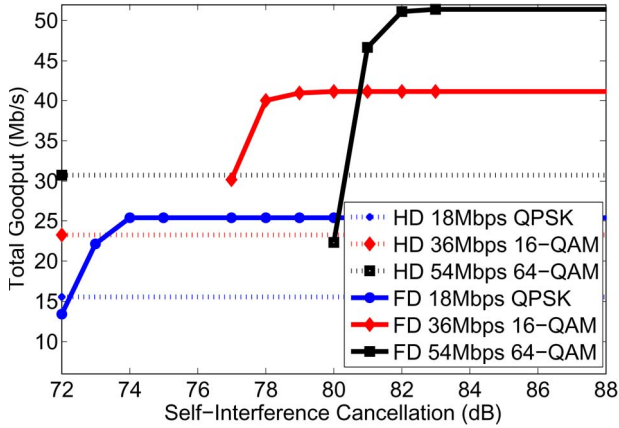


Fig. 9. Performance of different modulations and constellations versus self-interference cancellation, where HD system does not use RTS/CTS signaling.

study the system with a mix of full and HD nodes, where the HD nodes are legacy nodes, which do not ignore collisions in NAV duration.

Table IV provides the simulation parameters used. The self-interference cancellation values and modulation rates were varied for the results in Fig. 9. For other results, the self-interference cancellation was fixed at 85 dB (median value from experimental results) and modulation was fixed at 18-Mb/s QPSK to highlight the protocol dynamics. We used a path loss of 63 dBm, which corresponds to loss at a distance of 14 m and a frequency of 2.4 GHz using the free-space path loss formula ( $\text{path loss} = \lambda^2 / (16\pi^2 d^2)$ ) [25]. To model bit error rate, we assume that the self-interference and thermal noise are Gaussian, and we use the standard  $Q$ -functions for uncoded modulation [25]. The maximum packet size is 1500 bytes; there is no segmentation, and each packet is sent as the payload of one FD MAC frame.

#### A. Goodput Characterization for Different Packet Sizes

We evaluate FD MAC design for QPSK (18 Mb/s). The rate value, i.e., 18 Mb/s for QPSK, refers to the radio transmission rate. For a two-node system with one AP and one node STA, we compare an FD system against a legacy HD system with or without RTS/CTS. Total goodput is defined as the sum

of the goodput from the AP to the STA and from the STA to the AP. For HD 18-Mb/s QPSK, the total MAC goodput for HD system without RTS/CTS is 13.69 Mb/s, the total goodput for HD system with RTS/CTS is 12.8 Mb/s, whereas for FD, the MAC goodput is 25.62 Mb/s for packet size of 1500 bytes. Thus, there is an 87% performance gain for FD over HD system without RTS/CTS, including all MAC overheads and 100% gain for FD over HD system with RTS/CTS. While these gains are for symmetric traffic (equal packet sizes in the two directions), the following result holds in general.

*Result 7 (Gains of FD MAC):* FD goodput is *always* higher than HD goodput, for all asymmetric traffic, where the HD system may or may not use RTS/CTS.

Given that data traffic is predominantly based on TCP, an asymmetric TCP download-only traffic will have 1500 bytes from the AP to the STA (downlink) and 40 bytes of TCP ACK packets going from the STA to the AP (uplink). We model asymmetry by varying the size of the packets from the STA to the AP while keeping the cancellation fixed at 85 dB. We note that it is well recognized that the performance gain of FD is influenced by traffic asymmetry [27].

Table V shows that, as we increase the uplink packet size from 40 to 1500 bytes, FD provides a goodput gain ranging from  $1.3\times$  (13.14 versus 10.07) to  $2\times$  (25.62 versus 12.8), as compared with an HD system using RTS/CTS. The FD goodput is *always* higher than HD goodput, where the HD system may or may not use RTS/CTS. As the length of uplink data packet decreases, the uplink throughput decreases for an FD system, whereas the downlink throughput remains the same. We thus have  $(\text{uplink throughput}/\text{downlink throughput}) = (\text{uplink packet size}/\text{downlink packet size})$  for the FD system. In other words, the throughput divided by the size of data in each direction is constant. In an HD system, the time resource is shared by the two nodes, whereas in an FD system, the downlink transmission always happens and the uplink transmission can be viewed as a bonus.

We now compare the effect of varying self-interference cancellation in Fig. 9 assuming symmetric 1500-byte data in both directions. We note that as the self-interference cancellation improves, higher constellations can be supported for FD system, thus improving the rate. The rate for HD system does not depend on the self-interference cancellation. In the rest of this paper, we will mainly illustrate the results on 18-Mb/s QPSK constellation (1500-byte packet size) noting that the improvement factors will be similar at a fixed self-interference cancellation value of, for example, 83 dB.

#### B. Goodput Characterization for Multiple FD Nodes

Here, we consider the effect of scaling the network size to indicate multiple nodes with the packet sizes for all nodes being 1500 bytes.

*Result 8 (Gains for FD System With Multiple Nodes):* The sum throughput for an FD system with multiple nodes increases by a factor of approximately two when compared with an HD system with RTS/CTS handshake.

Consider the case when there are  $n$  FD nodes and one AP. In an 802.11 system, each node has equal chance of winning



TABLE V  
GOODPUT FOR VARYING PACKET SIZES, AP + 1 NODE, 85-dB CANCELCATION, THE GOODPUT NUMBERS ARE WRITTEN AS  
[GOODPUT FROM AP TO STATION (DOWNLINK), GOODPUT FROM STATION TO AP (UPLINK)]

AP-Node (bytes)	Node-AP (bytes)	HD w/o RTS (Mbps)	HD with RTS (Mbps)	FD (Mbps)	Gain (HD w/o RTS)	Gain (HD with RTS)
1500	1500	(6.92, 6.77)	(6.41, 6.39)	(12.81, 12.81)	1.87	2.00
1500	1000	(7.85, 5.26)	(7.21, 4.92)	(12.80, 8.54)	1.62	1.76
1500	500	(9.12, 3.05)	(8.38, 2.82)	(12.80, 4.27)	1.40	1.52
1500	40	(10.83, 0.3)	(9.81, 0.26)	(12.80, 0.34)	1.18	1.30

TABLE VI  
THEORETICAL NORMALIZED GOODPUT FOR DIFFERENT SCENARIOS (NORMALIZED TO THE SUM THROUGHPUT OF HD SYSTEM),  
WHERE THE NUMBER OF NODES  $n = 2m$ . CASE 1 IS THE CASE WITH MODIFIED HD NODES AS IN SECTION VII-C

Scenarios	Normalized Sum Goodput	Normalized Average Goodput per station		
		AP to HD node (HD downlink)	AP to FD node, FD node to AP (FD downlink=uplink)	HD node to AP (HD uplink)
$2m$ FD	2	-	$\frac{1}{n}$	-
$2m$ HD	1	$\frac{1}{n(n+1)}$	-	$\frac{1}{n+1}$
$m$ FD, $m$ HD Case 1	$1 + \frac{m}{n+1}$	$\frac{1}{m(n+1)}$	$\frac{1}{n+1}$	$\frac{1}{n+1}$

the channel contention due to random backoff; thus, each of the  $n + 1$  node accesses the channel with equal probability.

For comparison of FD and HD throughputs, we first ignore all timing and collision overheads and assume that all nodes have infinite queues that are always saturated and have data to be transmitted. Furthermore, the destination of each new arriving packet at the AP is uniformly distributed across all nodes. In an HD system, each node grabs the channel for a fraction  $1/(n + 1)$  time. When a node grabs the channel, it sends data to the AP, and thus, the fractional time slot used for data transfer from a node to the AP is  $1/(n + 1)$ . When the AP grabs the channel, it sends the data at the head of the queue to the appropriate node. Since the head of the queue can be addressed to any node with equally probability, the AP sends a packet to a node for  $1/(n(n + 1))$  of the time. The total throughput is normalized such that the sum throughput for the legacy HD system is 1.

For an FD system, each node grabs the channel for a fraction  $1/(n + 1)$  time. At each time, there are two concurrent communication paths ongoing, and thus, the normalized throughput is 2. The uplink throughput from any node and downlink throughput to any node is  $1/n$ , which means that each node transmits to the AP for  $1/n$  fraction of the time slots and *vice versa*. Thus, we see that FD improves the uplink throughput from a node from  $1/(n + 1)$  to  $1/n$ , which translates to an improvement factor of  $1 + 1/n$ . The downlink throughput to a node, on the other hand, improves from  $1/(n(n + 1))$  to  $1/n$ , an improvement by a factor of  $n + 1$ . Although the total throughput improves by a factor of 2, for  $n > 1$ , the downlink throughput to a node improves by a larger multiple, as compared with the uplink throughput from a node. The analysis here is summarized in the rows corresponding to FD and HD systems in Table VI.

The analysis ignored several aspects, e.g., collisions and different packet sizes. The HD system without RTS/CTS has collisions of data frames, whereas the FD system has collisions of RTS frames. The results from OPNET simulations provide realistic throughputs incorporating all overheads, as shown in Table VII. We report the sum goodput for the system together with average uplink and downlink goodputs. We

TABLE VII  
GOODPUTS WITH MULTIPLE NODES

Scenarios	Sum Goodput (Mbps)	Average Goodput (Mbps) AP to node (downlink)	node to AP (uplink)	% RTS/Data Collisions
$n = 1$				
FD	25.62	12.81	12.81	10.8
HD with RTS	12.8	6.41	6.39	11.1
HD without RTS	13.69	6.92	6.77	10.7
$n = 2$				
FD	26.02	6.52	6.52	8.1
HD with RTS	12.82	2.12	4.29	17.8
HD without RTS	13.25	2.13	4.49	17.8
$n = 4$				
FD	25.99	3.25	3.25	18.2
HD with RTS	12.78	0.67	2.53	26.9
HD without RTS	12.57	0.63	2.49	26.7
$n = 8$				
FD	25.6	1.6	1.6	32.3
HD with RTS	12.7	0.2	1.39	40.0
HD without RTS	11.8	0.16	1.31	35.8

also report collision statistics. For RTS packets in a system with RTS/CTS (e.g., percentage of RTS requests that collided as a percentage of total RTS transmissions), we have (percentage RTS collisions) =  $100 \times (\text{number of RTS packets that were not successfully received}) / (\text{total number of RTS packets sent including retransmissions})$ . Similarly, for HD system without RTS/CTS, the collision statistics are that for the DATA packet. We provide the percentage of collided data frames, which is the percentage of data packets not successfully received.

The ratio of (sum goodput for FD) to (sum goodput for HD) should be theoretically a factor of 2. We enumerate the ratio of sum goodput for the following cases: 2 for  $n = 1$ , 2.03 for  $n = 2$ , 2.03 for  $n = 4$ , and 2.02 for  $n = 8$ , when compared with an HD system with RTS/CTS. We note that the number of retransmissions for an FD system is much lower compared with that for an HD system with RTS/CTS, e.g., the number of RTS retransmissions reduces from 17.8% in the HD case for  $n = 2$  to 8.1% in the FD case.

We further observe that an HD system achieves better throughput with RTS/CTS than without RTS/CTS for  $n \geq 4$ .

TABLE VIII  
GOODPUTS WITH COEXISTENCE FOR MULTIPLE NODES WHERE IN CASE 1, HD NODES IGNORE COLLISIONS IN NAV, WHEREAS IN CASE 2, HD NODES ARE LEGACY AND DO NOT IGNORE COLLISIONS

Scenarios	Sum Goodput (Mbps)	Average Goodput (Mbps)		
		AP to HD node (HD downlink)	AP to FD node, FD node to AP (FD downlink=uplink)	HD node to AP (HD uplink)
$m = 1$				
$2m$ FD	26.07	-	6.52	-
$2m$ HD	12.82	2.12	-	4.29
$m$ FD, $m$ HD Case 1	17.87	3.81	4.81	4.45
$m$ FD, $m$ HD Case 2	18.64	4.79	5.65	2.55
$m = 2$				
$2m$ FD	25.99	-	3.25	-
$2m$ HD	12.78	0.67	-	2.53
$m$ FD, $m$ HD Case 1	18.15	1.37	2.59	2.54
$m$ FD, $m$ HD Case 2	20.59	1.67	3.78	1.07
$m = 4$				
$2m$ FD	25.6	-	1.6	-
$2m$ HD	12.7	0.2	-	1.39
$m$ FD, $m$ HD case 1	18.37	0.5	1.38	1.32
$m$ FD, $m$ HD case 2	21.86	0.59	2.23	0.42

RTS/CTS incurs timing overheads that reduce the system throughput. However, without RTS/CTS, a significant fraction of the time is wasted for recovering from the collisions of data frames, which degrade throughput more than the collisions of RTS frames. Thus, when  $n \geq 4$ , the collisions are high, the time saved by having RTS frame collisions instead of data frame collisions outweighs the overhead of RTS/CTS signaling. Consequently, we use an HD system with RTS/CTS as the baseline reference case for the rest of this paper.

From the discussion, the uplink throughput from a node is a factor  $n$  higher than the downlink throughput to a node for an HD system. We can observe in Table VII that factor  $n$  difference holds approximately for the HD system. We now compare the downlink throughput in FD and HD systems and note that, theoretically, the FD throughput should increase by a factor of  $n + 1$ . Based on the results, the gain of downlink throughput from an FD system compared with an HD system with RTS/CTS is a factor of 2, 3.08, 4.85, and 8 for  $n = 1, 2, 4$ , and 8 nodes, respectively, compared with the theoretical values of 2, 3, 5, and 9, respectively. For the uplink case, the throughputs of FD should increase by a factor of  $(n + 1)/n$  compared with an HD system. Our experimental results show an improvement factor of 2, 1.52, 1.28, and 1.15 for  $n = 1, 2, 4$ , and 8, respectively, as compared with the theoretical 2, 1.5, 1.25, and 1.13, respectively. Thus, we find that the simulation results match well with theory.

### C. Coexistence for FD and **Modified** HD Nodes That Ignore Collision During NAV

We examine the performance when legacy HD and FD nodes coexist within the same wireless LAN. Suppose that there are  $n = 2m$  nodes comprising  $m$  FD and  $m$  HD nodes. We first assume the case where the HD nodes use a modified MAC design. The modified version provides an insight into the dynamics of coexistence and also touches on an unfairness issue that we will highlight in the next section. Note that the modification may or may not be pragmatic in real scenarios.

We assume that the **modified** HD nodes ignore collisions during the NAV duration. Each node grabs the channel for a fraction  $1/(n + 1)$  time. When an HD node grabs the channel, it sends data to the AP. When an FD node grabs the channel, the AP also sends packets to the FD node. As a result, packets in the queue at AP for FD nodes get depleted faster than the HD nodes and do not have packets for FD node with probability 1 resulting in the AP always transmitting to HD nodes. (For more details on the proof of this statement, the reader is referred to [28].) Thus, the AP sends data to HD nodes for fraction  $1/(m(n + 1))$  time slots. The HD node sends data to AP for fraction  $1/(n + 1)$  time slots. Furthermore, FD node sends data to AP, and AP sends data to FD node for a fraction  $1/(n + 1)$  time slots.

Thus, the downlink throughput to the HD node increases from  $1/(n(n + 1))$  in a legacy HD system to  $1/(m(n + 1))$ , which is a factor-of-two improvement. The downlink throughput to the FD node increases from  $1/(n(n + 1))$  in a legacy HD system to  $1/(n + 1)$ , which is a factor  $n$  improvement. Furthermore, the uplink throughput from HD/FD node remains the same as a legacy HD system. The overall sum throughput is thus  $1 + m/(n + 1)$  factor more than the throughput of an HD system. These results are summarized as Case 1 in the coexistence case in Table VI.

*Result 9 (Coexistence With Modified HD Nodes):* In a mix of  $m$  FD and  $m$  HD nodes, the total throughput increases compared to an HD-only system by a factor of  $1 + m/(2m + 1)$ .

In Table VIII, we see the goodputs for the case when there are  $m$  FD and  $m$  HD nodes. Case 1 represents the case where the modified HD nodes avoid collisions during the NAV window. Note that the total throughput increases by a factor of 1.39, 1.42, and 1.45 for  $m = 1, 2$ , and 4, respectively, from the complete HD system, as compared with 1.33, 1.4, and 1.44 as predicted from the aforementioned theory.

Furthermore, we note that the uplink throughput from an FD node to the AP remains almost the same as the throughput from an HD node to the AP, in agreement with the previous

theoretical results. The downlink goodput to FD node is the same as the uplink goodput from FD node, which is also the same as the uplink goodput from a node in a legacy HD system. Finally, the downlink throughput to HD node should increase by a factor of 2 from the complete HD system. We note that throughput improvement factor from the simulations is 1.8 for  $m = 1$ , 2.05 for  $m = 2$ , and 2.5 for  $m = 4$ , comparable to the theoretical results.

#### D. Coexistence for FD and Legacy HD Nodes

Here, consider legacy HD nodes that will consider the FD exchange as a collision and therefore would wait for EIFS rather than DIFS after every FD transmission. The results for this scenario are shown in Table VIII, Case 2. When the HD nodes are legacy, we note that the FD nodes wait for DIFS, whereas the HD nodes wait for EIFS after the end of every FD transmission. The FD nodes thus obtain an unfair advantage in accessing the channel. Thus, the throughput from the HD node to the AP is reduced. Furthermore, packets for the FD node are removed from the queue at the AP faster, and when AP successfully gets the channel, it has packets remaining only for the HD node. Therefore, the downlink to HD nodes and the goodput from the AP to FD nodes increase when the HD nodes are legacy. Since FD transmissions happen for a larger time fraction, the overall sum goodput of the system increases. These results were generated when the buffer at the AP is large. When the buffer at AP is limited, AP may not have packets for FD node further limiting the throughput from AP to FD node; thus, the overall throughput reduces matching the performance closer to an HD system.

For the scenario with legacy HD nodes, we propose a coexistence-based MAC change for FD nodes such that the uplink throughput of HD node is not greatly impacted. The change for the FD nodes not involved in the FD exchange is to wait for EIFS for FD exchange similar to what the legacy HD nodes would be doing. The change for the FD nodes involved in the FD exchange is to wait for EIFS after every FD data exchange similar to what the legacy HD nodes would be doing. The change ensures that all nodes wait for DIFS before backoff after an HD packet exchange but wait for EIFS before backoff after an FD packet exchange. As a result, the FD nodes are more polite and do not get unfair advantage of repeatedly grabbing the channel. However, increased wait times after each FD transmission are slightly disadvantageous when there are a lot of FD nodes compared with legacy HD nodes since the FD nodes will wait longer (EIFS instead of DIFS). We note that the decrease in throughput due to extra wait time is not significant. The overall throughput for all FD nodes decreases from 25.6 to 25.05 Mb/s for  $n = 8$ , and the throughput for four FD and four HD systems reduces from the originally defined FD MAC and slightly modified HD MAC from 18.37 to 17.12 Mb/s for the “graceful” FD system with legacy HD system. Although the overall throughput decreases, the extra wait-time-based system does not compromise the legacy HD nodes’ uplink throughput significantly. Thus, we can summarize the main result of this section as follows.

*Result 10 (Coexistence of Modified FD and Legacy HD Nodes):* Overall, system throughput decreases with extra wait time for FD nodes, as compared to the coexistence between FD and modified HD nodes, but ensures minimal loss to legacy nodes’ throughput.

## VIII. CONCLUSION

This paper has presented the first design for an FD multi-antenna 20-MHz WiFi-ready design. We achieved the best self-interference cancellation reported to date and presented an integrated PHY and MAC design that is compatible with IEEE 802.11x, enabling accelerated adoption of FD wireless. Our design achieves high rate and extended range, adequate for most indoor WiFi deployments.

## REFERENCES

- [1] S. Chen, M. A. Beach, and J. P. McGeehan, “Division-free duplex for wireless applications,” *Electron. Lett.*, vol. 34, no. 2, pp. 147–148, Jan. 1998.
- [2] A. K. Khandani, “Methods for spatial multiplexing of wireless two-way channels,” U.S. patent 7817641, Oct. 19, 2010, filed Oct. 2006 (provisional patent filed Oct. 2005).
- [3] D. W. Bliss, P. Parker, and A. R. Margetts, “Simultaneous transmission and reception for improved wireless network performance,” in *Proc. IEEE/SP 14th Workshop Stat. Signal Process.*, Aug. 2007, pp. 478–482.
- [4] B. Radunovic, D. Gunawardena, P. Key, A. P. N. Singh, V. Balan, and G. Dejean, “Rethinking indoor wireless: Low power, low frequency, full duplex,” in *Proc. 5th IEEE Workshop Wireless Mesh Netw.*, 2010, pp. 1–6.
- [5] J. Choi, M. Jain, K. Srinivasan, P. Levis, and S. Katti, “Achieving single channel, full duplex wireless communication,” in *Proc. ACM Mobicom*, 2010, pp. 1–12.
- [6] M. Duarte and A. Sabharwal, “Full-duplex wireless communications using off-the-shelf radios: Feasibility and first results,” in *Proc. Asilomar Conf. Signals, Syst., Comput.*, 2010, pp. 1558–1562.
- [7] M. Jain, J. Choi, T. M. Kim, D. Bharadia, S. Seth, K. Srinivasan, P. Levis, S. Katti, and P. Sinha, “Practical, real-time full duplex wireless,” in *Proc. ACM Mobicom*, 2011, pp. 301–312.
- [8] A. Sahai, G. Patel, and A. Sabharwal, “Pushing the limits of full-duplex: Design and real-time implementation,” Rice Univ., Houston, TX, USA, Rep. TREE1104, 2011.
- [9] A. Sahai, G. Patel, and A. Sabharwal, “Asynchronous full-duplex wireless,” in *Proc. IEEE COMSNETS*, Jan. 2012, pp. 1–9.
- [10] M. A. Khojastepour, K. Sundaresan, S. Rangarajan, X. Zhang, and S. Barghi, “The case for antenna cancellation for scalable full duplex wireless communications,” in *Proc. Hotnets*, Nov. 2011, p. 17.
- [11] E. Aryafar, M. A. Khojastepour, K. Sundaresan, S. Rangarajan, and M. Chiang, “MIDU: Enabling MIMO Full Duplex,” in *Proc. ACM Mobicom*, 2012, pp. 257–268.
- [12] *SMA attenuator*, Pasternack Enterprises, Irvine, CA, USA, Data Sheet.
- [13] *SMA female power divider PE2014*, Pasternack Enterprises, Irvine, CA, USA, Data Sheet.
- [14] *Wireless Open-Access Research Platform (WARP)*. [Online]. Available: <http://warpproject.org/trac>
- [15] S. M. Alamouti, “A simple transmit diversity technique for wireless communications,” *IEEE J. Sel. Areas Commun.*, vol. 16, no. 8, pp. 1451–1458, Oct. 1998.
- [16] *Communications System Toolbox R2011b*, MIMO, Natick, MA, USA.
- [17] *2.4 GHz 7 dBi Desktop Omni Antenna Spec.* [Online]. Available: <http://www.l-com.com>
- [18] M. Duarte, “Full-duplex wireless: Design, implementation and characterization,” M.S. thesis, Dept. Electr. Comput. Eng., Rice University, Houston, TX, USA, 2012.
- [19] T. Riihonen, S. Werner, and R. Wichman, “Mitigation of loopback self-interference in full-duplex MIMO relays,” *IEEE Trans. Signal Process.*, vol. 59, no. 12, pp. 5983–5993, Dec. 2011.
- [20] M. Duarte, C. Dick, and A. Sabharwal, “Experiment-driven characterization of full-duplex wireless systems,” *IEEE Trans. Wireless Commun.*, vol. 11, no. 12, pp. 4296–4307, Dec. 2012.
- [21] D. Tse and P. Viswanath, *Fundamentals of Wireless Communications*. Cambridge, U.K.: Cambridge Univ. Press, 2005.



- [22] W. Kim, H. Lee, M. Kim, and H. K. Chung, "Distribution of eigenvalues for  $2 \times 2$  MIMO channel capacity based on indoor measurements," *IEEE Trans. Wireless Commun.*, vol. 11, no. 4, pp. 1255–1259, Apr. 2012.
- [23] J. Geier, 802.11 Medium Access Methods, Nov. 2002. [Online]. Available: <http://www.wi-fiplanet.com/tutorials/article.php/1548381>
- [24] M. Duarte, A. Sabharwal, V. Aggarwal, R. Jana, K. K. Ramakrishnan, C. Rice, and N. K. Shankaranayanan, Design and characterization of a full-duplex multi-antenna system for WiFi networks, Oct. 2012. [Online]. Available: <http://arxiv.org/pdf/1210.1639v2.pdf>
- [25] J. G. Proakis, *Digital Communications*. New York, NY, USA: McGraw-Hill, 1983.
- [26] *IEEE Standard for Information Technology–Telecommunications and Information Exchange Between Systems–Local and Metropolitan Area Networks–Specific Requirements—Part 11: Wireless LAN Medium Access Control (MAC) and Physical Layer (PHY) Specifications*, IEEE Std 802.11-2007, Jun. 2007.
- [27] N. Singh, D. Gunawardena, A. Proutiere, B. Radunovic, H. V. Balan, and P. Key, "Efficient and fair MAC for wireless networks with self interference cancellation," in *Proc. WiOpt*, Princeton, NJ, USA, 2011, pp. 94–101.
- [28] V. Aggarwal and N. K. Shankaranayanan, "Performance of a random-access wireless network with a mix of full- and half-duplex stations," *IEEE Commun. Lett.*, 2013, to be published. [Online]. Available: <http://ieeexplore.ieee.org/xpl/articleDetails.jsp?tp=&arnumber=6626310>
- [29] [Online]. Available: <http://www.opnet.com>



**Melissa Duarte** (M'12) received the B.S. degree in electrical engineering from the Pontificia Universidad Javeriana, Bogota, Colombia, in 2005 and the M.S. and Ph.D. degrees in electrical and computer engineering from Rice University, Houston, TX, USA, in 2007 and 2012, respectively.

She is currently a Postdoctoral Researcher with the School of Computer and Communication Sciences, École Polytechnique Fédérale de Lausanne, Lausanne, Switzerland. Her research interests include the design and implementation of architectures

for next-generation wireless communications.



**Ashutosh Sabharwal** (S'91–M'99–SM'04) received the B.Tech. degree from the Indian Institute of Technology Delhi, New Delhi, India, in 1993 and the M.S. and Ph.D. degrees from The Ohio State University, Columbus, OH, USA, in 1995 and 1999, respectively.

He is currently a Professor with the Department of Electrical and Computer Engineering, Rice University, Houston, TX, USA. His research interests include information theory, communication algorithms, and experiment-driven design of wireless

networks.

Dr. Sabharwal received the 1998 Presidential Dissertation Fellowship Award.



**Vaneet Aggarwal** (S'08–M'11) received the B.Tech. degree from the Indian Institute of Technology Kanpur, Kanpur, India, in 2005 and the M.A. and Ph.D. degrees from Princeton University, Princeton, NJ, USA, in 2007 and 2010, respectively, all in electrical engineering.

He is currently a Senior Member of the Technical Staff with AT&T Labs Research, Florham Park, NJ, USA, and an Adjunct Assistant Professor with Columbia University, New York, NY, USA. His research interests are in the applications of information

and coding theory to wireless systems and distributed storage systems.

Dr. Aggarwal received the Princeton University's Porter Ogden Jacobus Honorable Fellowship in 2009.



**Rittwik Jana** (M'90) received the Bachelor's degree in electrical engineering from The University of Adelaide, Adelaide, Australia, in 1994 and the Ph.D. degree from the Australian National University, Acton, Australia, in 1999.

From 1996 to 1999, he was an Engineer with the Defense Science and Technology Organization, Australia. Since 1999, he has been a Principal Member of the Technical Staff with AT&T Labs Research, Florham Park, NJ, USA. His research expertise falls in the areas of Internet Protocol television, peak-to-

peak, mobile middleware, and wireless channel modeling.



**K. K. Ramakrishnan** (F'05) received the M.S. degree from the Indian Institute of Science, Bangalore, India, in 1978 and the M.S. and Ph.D. degrees in computer science from the University of Maryland, College Park, MD, USA, in 1981 and 1983, respectively.

He joined AT&T Bell Laboratories in 1994 and has been with AT&T Labs Research, Florham Park, NJ, USA, since its inception in 1996. Prior to 1994, he was a Technical Director and Consulting Engineer in networking with Digital Equipment Corporation.

Between 2000 and 2002, he was with TeraOptic Networks, Inc., as Founder and Vice President. A Distinguished Member of Technical Staff with AT&T Labs Research, he is involved in several technical and strategic activities in networking and information distribution. He has published nearly 200 papers and has more than 120 patents issued in his name.

Dr. Ramakrishnan is an AT&T Fellow, recognized for his contributions to communication networks, including congestion control, traffic management, and virtual private network services. He has been a member of the National Research Council Panel on Information Technology for the National Institute of Standards and Technology. He is with the Editorial Board of *Networking Science* and has been on the Editorial Board of the IEEE/Association for Computing Machinery TRANSACTIONS ON NETWORKING and *IEEE Network Magazine*.



**Christopher W. Rice** received the B.S.E.E. and M.S.E.E. degrees (*summa cum laude*) from Virginia Polytechnic Institute and State University, Blacksburg, VA, USA, and the M.B.A. degree from the University of Central Florida, Orlando, FL, USA, while working full time.

He is Vice President of AT&T Labs Research, Florham Park, NJ, USA, where he is responsible for leading research in areas, including big data, network and service performance research, and new IP services platform research. He successfully launched

several services into the marketplace based on his research and has more than 30 patents in his name.

Mr. Rice received the AT&T Distinguished Scientist Award in 2005.



**N. K. Shankaranarayanan** (S'83–M'92–SM'98) received the B.Tech. degree from the Indian Institute of Technology Bombay, Mumbai, India, in 1985, the M.S. degree from Virginia Polytechnic Institute and State University, Blacksburg, VA, USA, in 1987, and the Ph.D. degree from Columbia University, New York, NY, USA, in 1992, all in electrical engineering.

During 1991, he was a Visiting Researcher with the University of California, Berkeley, CA, USA. Since 1992, he has been with several research orga-

nizations of AT&T (Bell) Laboratories and has worked on a diverse range of broadband technologies with a focus on improving the end-to-end performance experience enjoyed by the end user. His research work has spanned service and technology aspects of cellular, WiFi, fixed wireless, cable, and optical networks. He was part of the core team that deployed the first two-way broadband wireless field system in 1997. During 2006–2008, he served as an AT&T Board Member, Chair of the Service Provider Working Group and Chair of the X.509 Certificate Task Force at the WiMAX Forum. He is currently a Principal Member of the Technical Staff-Research with the Service Quality Management Department, AT&T Labs Research, Bedminster, NJ, USA. He has more than 20 patents in his name. His current work is focused on service quality management in deployed networks, improving end-to-end user performance in Third-Generation/Fourth-Generation cellular and WiFi networks, and experimental and simulation prototypes of mobility networks.